

PERFORMANCE TUNING OF IC ENGINE WITH VARIABLE EXHAUST SYSTEM
USING A ONE-D SIMULATION TOOL

by

Vineeth Gajula

A thesis submitted to the faculty of
The University of North Carolina at Charlotte
in partial fulfillment of the requirements
for the degree of Master of Science in
Mechanical Engineering

Charlotte

2017

Approved by:

Dr. Saiful Bari

Dr. Mesbah Uddin

Dr. Peter T. Tkacik

ABSTRACT

VINEETH GAJULA, Performance tuning of IC engine with variable exhaust system using a one-D simulation tool. (Under the direction of DR. SAIFUL BARI)

The exhaust system has a significant effect on the breathing capability of an IC engine, which when increased, increases the volumetric efficiency. Due to the sudden opening of the exhaust valve, the highly pressurized gases in the combustion chamber rush out creating a pressure wave. When the low pressure wave is made to return at the time of exhaust valve opening, the evacuation of exhaust gases improve. This is due to the higher pressure differential that is created by the low pressure wave. Using this principle, the exhaust system was tuned with a one-D simulation tool to achieve higher scavenging efficiency. However, as the engine speed changes the requirements to achieve the tuned condition changes and also the strength of the wave decreases for every reflection. With a variable runner length system the higher engine speeds use the first reflection and lower engine speeds are shifted to use later low pressure wave reflections. Tuning the exhaust valve timing along with the runner length further improved the performance. With tuned runner length and valve timing 1-2% and 5-8% improvement was seen in brake torque at higher and lower engine speeds respectively. Increase in valve lift, where low pressure wave is taken advantage of, increased torque by another 1-2%. However, when the compression wave returns at EVO, low lift reduced the negative effect of the compression wave. With 20% less lift, almost 50% of the loss incurred due to shifting between reflections was reduced. Overall, 2-3% and 7-10% improvement in torque was achieved with variable runner length and valve train system at higher and lower engine speeds respectively.

ACKNOWLEDGMENTS

The success and final outcome of my thesis required a lot of guidance and assistance from many people. I thank them whole heartedly for their continued support until the completion of my work. Such help was very crucial for my achievements in this thesis.

I respect and thank Dr. Saiful Bari for providing me an opportunity to do the work on IC Engine Exhaust Systems and giving me all support and guidance which made me complete the thesis duly. I am extremely thankful to him for providing such support although he had a busy schedule.

I am thankful for the support and guidance from the professors and staff from the Mechanical Engineering Department, which helped me in successfully completing my work. Also, I would like to extend my sincere esteems to all staff in Motorsports Research Laboratory for their timely support.

I owe my gratitude to other research partners, who worked closely and engaged in healthy discussions. I thank my fellow students for their encouragement.

Vineeth Gajula

TABLE OF CONTENTS

LIST OF TABLES	viii
LIST OF FIGURES	ix
LIST OF ABBREVIATIONS	xii
CHAPTER 1: INTRODUCTION	1
1.1. WAVE THEORY	2
1.2. RICARDO WAVE	7
CHAPTER 2: METHODOLOGY	9
2.1. CREATING A 1-D MODEL	11
2.1.1. FUEL SETUP	12
2.1.2. AMBIENT CONDITIONS	13
2.1.3. CREATING JUNCTIONS	14
2.1.4. DUCTS AND DISCRETIZATION	15
2.1.5. Y-JUNCTIONS	15
2.1.6. DUCT INITIAL CONDITIONS	17
2.1.7. BUTTERFLY VALVE	19
2.1.8. ENGINE SETUP	20

2.1.9. CONSTANTS	23
2.1.10. COMBUSTION MODEL	24
2.1.11. HEAT TRANSFER MODEL	24
2.1.12. POPPET VALVES	25
2.2. VALIDATION OF THE MODEL	27
2.3. CASE SETUP	29
CHAPTER 3: RESULTS AND DISCUSSIONS	33
3.1. INITIAL STUDY WITH RUNNER LENGTH AND VALVE TIMING	33
3.1.1. EXHAUST RUNNER LENGTH	33
3.1.2. REFLECTIONS	39
3.1.3. EXHAUST VALVE TIMING	41
3.1.4. OBSERVATIONS	44
3.2. BASIS FOR FURTHER STUDY	47
3.2.1. VARIATION OF RUNNER LENGTH	48
3.2.1.1. REFLECTIONS AND PULSE STRENGTH	53
3.2.1.2. RUNNER LENGTH SELECTION	54
3.2.2. VARIATION OF VALVE OPENING TIME AND LIFT	57

3.2.3. IMPROVEMENTS	64
CHAPTER 4: CONCLUSION	67
REFERENCES	70

LIST OF TABLES

TABLE 1: Engine specifications and operating conditions	10
TABLE 2: Recommended values for Chen-Flynn correlation model	22
TABLE 3: Comparison of the performance for the two segment lengths	38
TABLE 4: Comparison of exhaust gas flow for 560 mm and 880 mm runner lengths for 3000 RPM	53

LIST OF FIGURES

FIGURE 1: Exhaust runner length calculations based on Equations (2) & (3)	5
FIGURE 2: Ricardo Wave window with blank canvas	11
FIGURE 3: Fuel and air properties window with Indolene fuel tag selected	12
FIGURE 4: Air inlet ambient atmosphere properties window	14
FIGURE 5: Dimension window for diffuser connecting restrictor to plenum	16
FIGURE 6: Relation between discretization and results	17
FIGURE 7: Exhaust runner editor window	18
FIGURE 8: Initial conditions set for exhaust runner	18
FIGURE 9: Dynamic display of the orifice element on canvas	19
FIGURE 10: Throttle valve editor window	20
FIGURE 11: Engine cylinder dimension window	21
FIGURE 12: Engine general panel window	23
FIGURE 13: Combustion sub-model window	25
FIGURE 14: Exhaust valve profile as shown in Ricardo Wave based on user input	26
FIGURE 15: 1-D model as prepared in Ricardo Wave	26

FIGURE 16: Engine Torque (N-m) and Engine Power (hp) comparison between simulation and chassis dynamometer	28
FIGURE 17: Time plot editor window for pressure sensor in exhaust port	30
FIGURE 18: Case setup for runner length, valve timing and lift variations in exhaust system	32
FIGURE 19: Torque values at different engine speeds for different lengths	34
FIGURE 20: Engine torque deficiency plot for all engine speeds for all the lengths analyzed	35
FIGURE 21: Engine torque for different lengths for 3500 RPM	37
FIGURE 22: Pressures traces in exhaust port near exhaust valve and intake mass flow (kg/s) at intake valve for 3500 RPM	38
FIGURE 23: Engine torque at a 1500 RPM for different lengths	39
FIGURE 24: Sequence of lengths that can be chosen limiting it to 600 mm	41
FIGURE 25: Engine torque at 1000 RPM for different valve timings	42
FIGURE 26: Engine torque at 4500 RPM for different valve timings	42
FIGURE 27: Engine torque at 7000 RPM for different valve timings	43
FIGURE 28: Sequence of valve timings that can be chosen	43
FIGURE 29: Improvement possible by having a totally variable length system	45
FIGURE 30: Improvement possible by having a limited variable length system	45
FIGURE 31: Percentage improvement with totally variable length system	46
FIGURE 32: Percentage improvement with limited variable length system	46

FIGURE 33: Engine torque (Nm) Vs Runner length (mm) and Engine speed (RPM)	48
FIGURE 34: Engine torque (Nm) Vs Runner length for 3000 RPM	49
FIGURE 35: Pressure traces at approx. 9mm downstream from exhaust valve for the two runner lengths	50
FIGURE 36: Intake mass flow rate (kg/s) for the two runner lengths	50
FIGURE 37: Difference of maximum and achieved engine torque at runner length for each engine speed	56
FIGURE 38: Engine torque for variable sequence runner length	56
FIGURE 39: 3D surface plot of engine torque for engine speed of 2000 RPM	58
FIGURE 40: Engine torque variation with changes in valve timing for engine speed of 2000 RPM for different runner lengths	60
FIGURE 41: Variation of engine torque with variation of exhaust valve lift for 7000 RPM	62
FIGURE 42: Pressure traces 9 mm downstream of exhaust valve and mass flow rate at exhaust valve for 7000 RPM for valve lift of 0.8X and 1.2X	63
FIGURE 43: Engine Torque improvements with exhaust valve timing and lift	65
FIGURE 44: Percentage improvements with variable exhaust system	66

LIST OF ABBREVIATIONS

1-D	One Dimensional
3D	Three Dimensional
aBDC	after BDC
aTDC	after TDC
bBDC	before BDC
BDC	Bottom Dead Center
bTDC	before TDC
CA	Crank angle
EVC	Exhaust Valve Closing
EVO	Exhaust valve opening
FMEP	Frictional Mean Effective Pressure
IC	Internal Combustion
IVC	Inlet Valve Opening
IVO	Inlet Valve Closing
K	Kelvin
mm	millimeter
ms	millisecond
RPM	Revolutions per Minute

CHAPTER 1: INTRODUCTION

It is true that the intake system has much stronger effect of engine breathing, but, the exhaust system too has a significant effect of the performance of an engine. Major studies are being done on the flow of gases in intake systems. It is well known that the intake system affects the engine's breathing capability, and thus has an effect on the resulting engine performance [1, 2]. The intake system has direct effect on the amount of air that enters the combustion chamber [3, 4]. Newer technologies are being developed and seen in most regular passenger cars as a standard feature. Whereas, very little development has taken place in improving the exhaust gas evacuation, which would indirectly help to gain higher volumetric efficiencies. The exhaust gases need to evacuate quickly to allow more volume and less hindrance for the intake charge to flow in [5]. Intake and exhaust systems as a pair can yield enormous improvements [6]. However, the exhaust system alone can itself gain significant improvement in engine breathing and thus its performance [7].

Developments in IC engine exhaust system and its tuning have been studied from over 65 years [8-11]. During this period, research had shown that the exhaust system has substantial influence on the performance of the engine. The exhaust system affects the evacuation of the burnt gases, which is defined as the scavenging efficiency. The higher the scavenging efficiency lesser is the residual fraction and also higher volumetric efficiency is achieved. A higher volumetric efficiency means higher performance of the engine and thus produces more power and torque [12]. Therefore, proper understanding

of the relation of the exhaust system with such factors helps in gaining more performance from an IC engine [13, 14]. Unsteady engine gas flow within the intake and exhaust runners has been a fascinating area for many engineers due to its potential for improving the performance of the engine [15-17].

1.1. WAVE THEORY

Post combustion in the cylinder during the power stroke, when the exhaust valve opens, the highly pressured gases in the cylinder start to rush out through the exhaust valve. This creates a high local pressure wave. Pressure waves have their own physics. This high pressure wave generated at the exhaust valve travels through the uniform exhaust runner. The pressure wave keeps flowing until it sees a change in the flow area [18]. For an exhaust system, the runners would see the change in flow area when connects to collector, muffler or to atmosphere. The high pressure wave when sees the change in flow area at the end of the runner, it reflects back. Since there is a change in the flow area, based on the physics of the pressure waves, the high pressure wave is converted to a low pressure wave. The low pressure wave starts flowing through the runner back towards the exhaust valve.

The low pressure wave when reaches the exhaust valve, if the exhaust valve is closed, the wave reflects against the exhaust valve. Since, there is no change in the flow area, the low pressure remains as a low pressure wave and starts flowing towards the end of the runner. The low pressure wave when reaches the end of the runner, where the flow area changes it reflects back as a high pressure wave. The high pressure waves travels

back towards the exhaust valve and reflects against the closed valve still as a high pressure wave. This process of reflections - with change of sign at the runner end and same sign at the exhaust valve - continues until the exhaust valve is opened and a new pressure wave is created. The high pressure wave is also called a compression wave and the low pressure wave is also called a rarefaction wave. These reflections can be an advantage or a disadvantage to the evacuation of exhaust gases.

$$c = \sqrt{kRT} \quad (1)$$

where, c = speed of sound (m/s)

k = specific heat ratio

R = gas constant (286 J/kg-K)

T = gas temperature (K)

The pressure waves flow at the speed of sound [19] given by Equation (1). The exhaust gases are very hot and speed of sound at these temperatures is nearly 600 m/s. The time for the pressure waves to return after one reflection will depend on how much time it takes for the exhaust valve to open again in the following cycle. The exhaust valve opens every 2 revolutions or 720° CA rotation. If the runner lengths can be tuned in such a way that the low pressure waves return to the exhaust valve when it opens, the pressure differential is higher. Higher the pressure differential, higher would be the scavenging effect and thus the exhaust gases expel out more efficiently. Say at an engine speed of 3000 RPM, 720° CA rotation takes 40 ms and at 6000 RPM it takes only 20 ms. Therefore, the runner length at 6000 RPM needs to be only half the runner length at 3000

RPM for first reflection. This suggests that as the conditions change and as engine speed changes, the runner length required keeps changing.

The theory of pressure waves are known from many years and have being used well in the intake systems. A number of formulae and theories exist for the intake system such as Helmholtz Resonator, David Vizard's Rule [20], Engelmann's Formula [21], etc. for hand calculations of required intake runner lengths. There are a few generalized wave travel time-distance equations but very little specifically for IC engine exhaust systems. Blair et al. [15] proposed an exhaust tuning coefficient, shown in Equation (2), for calculating the required exhaust runner length based on the mean exhaust gas temperature and engine speed. Bell et al. [22] proposed an equation, given by Equation (3), to calculate the runner length required in inches based on exhaust valve opening time and engine speed. Both these equations for hand calculations are a good starting point determine the runner length required at various engine speeds.

$$L_{et} = \frac{C_{et}\sqrt{T_{ex}+273}}{N} \quad (2)$$

where, L_{et} = tuned length of straight pipe (mm)

C_{et} = exhaust tuning coefficient = 2.058×10^5

T_{ex} = mean exhaust gas temperature (°C)

N = engine speed (rpm)

$$L_{in} = \left[\frac{850(360-EVO)}{rpm} \right] - 3 \quad (3)$$

Where, L_{in} = primary pipe length in inches

EVO = exhaust valve opening time

rpm = engine speed tuned for

For the two equations given by Blair et al. and Bell et al., if the calculated values are plotted, Figure 1 is obtained. The two curves are very close to each other and follow a similar trend. The runner length required for 11000 RPM is around 400 mm for Equation (2) and about 550 mm for Equation (3). As the engine speed decreases the runner length requirement increases. For about 6000 RPM, the length required is around 850 mm for Equation (2) and about 1000 mm for Equation (3). The runner length requirement then increases steeply from 6000 RPM to 3000 RPM and rises exponentially as the engine speed further decreases. The runner length requirement at 1000 RPM is about 5300 mm for Equation (2) and about 6100 mm for Equations (3). Such long lengths are practically not feasible for packaging in an engine. Lengths up to 1000 mm are probably the higher limit to which the runners can be packaged. Therefore, limiting the analysis to 1000 mm is an ideal range.

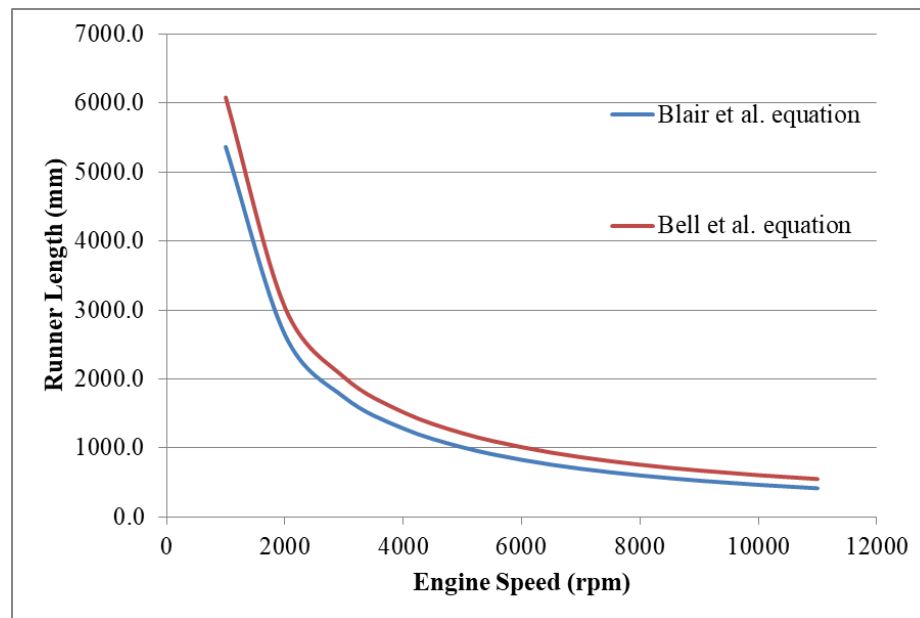


FIGURE 1: Exhaust runner length calculations based on Equations (2) & (3)

Sammur et al. varied the intake and exhaust runner in steps of 0.1 m and also the valve timings on the effects of the volumetric efficiency of a single cylinder engine [23]. Their results show considerable changes of 5-10% improvement in volumetric efficiency with changes in length. The analysis shows that different runner lengths benefit at different engine speeds. In other words, one runner length is beneficial for only one engine speed. Therefore, to obtain better performance at different engine speeds, different runner lengths are required. The intake or exhaust runner length is a function of the engine speed. Ohata et al. observed that the volumetric efficiency stays constant until the pulse timing was in the neighborhood of BDC and IVC at the end of intake stroke [24]. Bush et al found that a low-pressure (rarefaction) wave arriving at valve overlap period produced maximum benefit [25].

Unsteady gas flow in both intake and exhaust systems has been a fascinating area for many engineers. Due to complexity of flow in these systems, a lot of recent studies were computational studies [26-28]. For research, engineers were using privately developed or commercially available softwares for simulations. These were able to accurately predict the dynamics of the waves in both systems. With these tools, researchers and engineers were able to study the effects on the systems with little or without any physical work [29]. They were able to approach the design process in a much quicker and less expensive way and start at near optimum range. Such simulation tools also enable for study with more number of cases and without any practical or manufacturing limitations that would otherwise exist in physical experiments. Simulation tools are used in automotive industry in several areas, including vehicle dynamics, electrical, aerodynamics, etc. [30] . It is easier to analyze the results in simulation

softwares with multiple changes and to understand the pattern or behavior with these changes.

Before the actual testing, engine simulation tools are a worthy means to tune the exhaust system as well other engine design parameters which is a cost effective method before any physical tests may be performed [15, 31-33]. Ohata et al. [24] benefits from the flexibility of a 1-D simulation for the intake system and made it possible to identify the optimum conditions which generated a tuned condition in the intake system with the help of the simulation tool. Bush et al. [25] employed a similar approach in the exhaust and Blair et al. [15] utilized a 1-D engine simulation to split the forward and the backward moving wave in the exhaust to give a better understanding of the reflected wave and its effect on the pressure history in the exhaust port.

1.2. RICARDO WAVE

Ricardo developed an engineering code, for studying 1-D gas dynamics and engine simulation, called Wave. It is market leading ISO approved software used in many industries worldwide, including passenger car, motorcycle, truck, locomotive, motor sport, marine and power generation [34]. The 3D data, engine related data and operating conditions are the inputs to the software and it converts these into a 1-D model. This 1-D model along with several pre-existing and user defined sub-models creates an output file with the software's strong computational methods. It provides a fully integrated treatment of time-dependent fluid dynamics and thermodynamics. Based on the output generated by the software, the dynamics of pressure waves, mass flows, energy losses, heat transfer,

etc. can be analyzed in ducts, plenums, manifolds, etc. [34]. Based on the preprocessing and post processing options, the output data can be used to see volumetric efficiency, power, torque, emissions fuel consumption and so on.

The strength of the software is in the number of inbuilt sub-models that are available. It has models for calculating pressure, force, momentum, mass transfer, heat transfer, combustion, friction, etc. For friction calculations, IRIS and Chen-Flynn models are available, where the later is known for its accurate friction predictions in engines. For combustion, SI Wiebe, Diesel Wiebe and other models are available which predicts the duration for burning certain fraction of air-fuel mixture. If the data from an engine dynamometer is available, a user defined model can be used as well. Woschni, Colburn, Annand and other models are available for heat transfer calculations. Woschni model does consider the changes in the gas temperatures to calculate its speed, whereas Annand model simply considers the speed of gas to be equal to the mean piston speed. For turbulence and flow, Axisymmetric swirl and 3-Axis flow prediction models are available.

CHAPTER 2: METHODOLOGY

For this research, a single cylinder engine four stroke gasoline engine is selected. A single cylinder engine enables to observe the effect of the changes in the exhaust system as there would be no interference from other cylinders. The engine is a 510.4 cc displacement engine used on a dirt bike, KTM 500EXC. The engine has a high compression ratio of 11.8, which would generate a larger magnitude of effects being studied. The engine has four valves, two for the intake and two for the exhaust. Such valve configuration has a good flow rate and better exchange of air through the combustion chamber and therefore would help in the study as the pressure wave theory is based on the flow of air. A 1-D model is created for this engine based on its dimensions and operating conditions [35]. Unknown dimensions are measured as required, such as the valve diameters and their lift profiles. The ideal operating conditions are used for all analysis, 300 K for ambient air temperature and 1 bar atmospheric pressure. The dimensions of engine and other parameters used for the 1-D model are given in Table 1.

TABLE 1: Engine specifications and operating conditions

Displacement	510.4 cc	
Bore	95 mm	
Stroke	72 mm	
Clearance height	2 mm	
Connecting rod length	122.4 mm	
Compression ratio	11.8	
Ambient air temperature	300 K	
Atmospheric pressure	1 bar	
Fuel type	Indolene	
Heat transfer model	Woschni	
Combustion model	SI Wiebe	
	Intake system	Exhaust system
Number of valves	2	2
Valve diameter	40 mm	33 mm
Valve lift	9.7 mm	8.6 mm
Valve opening time	13° bTDC	71° bBDC
Valve closing time	70° aBDC	44° aTDC
Runner diameter	38 mm	46 mm

2.1. CREATING A 1-D MODEL

Ricardo Wave has different tools for building the 1-D model and for post-processing the output. For building the 1-D model, WaveBuild is used. WaveBuild interface includes a canvas, modelling tools and several other options. When the software is opened, it consists of a blank canvas where items can be dragged to build a 1-D model very easily. Ricardo Wave window along with the blank canvas is shown in Figure 2. The canvas is the main area where the flow network is created and assembled. Canvas is a customizable surface and the properties like canvas size, annotation display and grid appearance can be changed by selecting canvas properties. The unit system is set to SI unit system in simulation control. However, the units system for each input is displayed beside the entry field and the input can be entered in a different unit system.

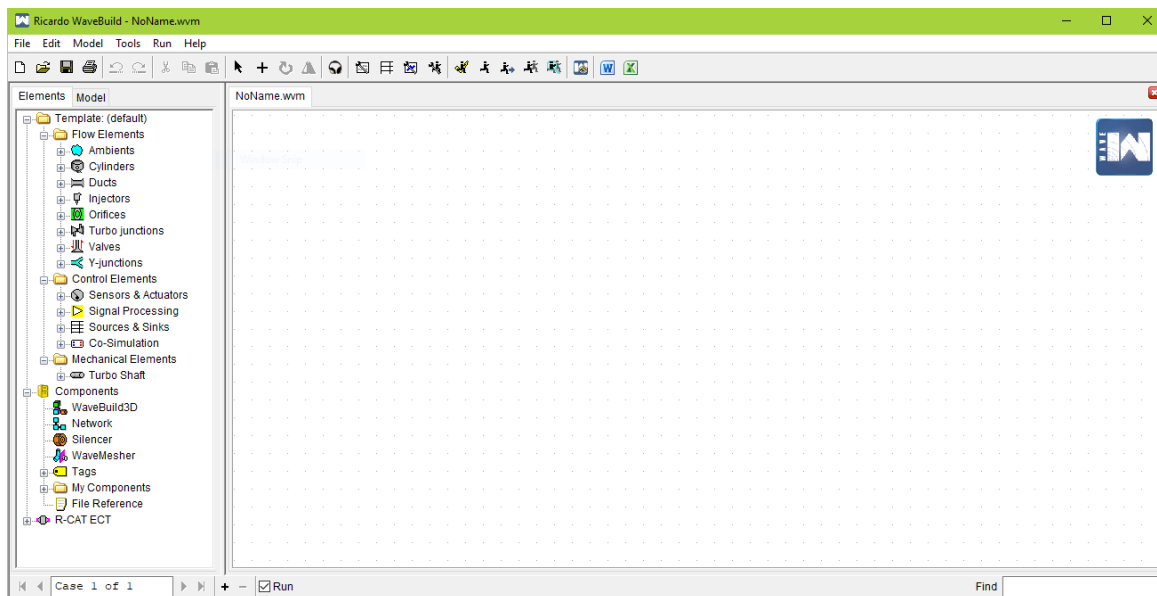


FIGURE 2: Ricardo Wave window with blank canvas

2.1.1. FUEL SETUP

In the fuel and air section, Indolene fuel tag is selected as the fuel type, shown in Figure 3. Indolene also known as E0 is chosen as the fuel type which is considered neat gasoline and provides a more uniform basis of comparison [36]. In WAVE, five types of species are transported throughout the model. They are fresh air, vaporized fuel, burned air, burned fuel and liquid fuel. All appropriate properties of these species are given in the fuel tag file which defines how fuel and air react at different temperature, pressures and concentrations.

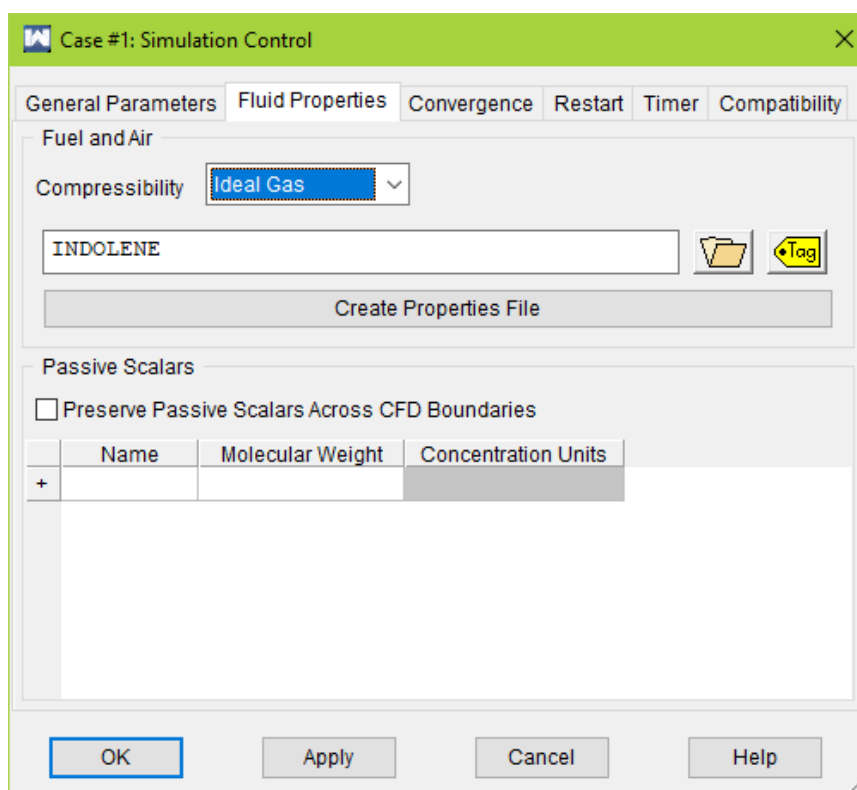


FIGURE 3: Fuel and air properties window with Indolene fuel tag selected

2.1.2. AMBIENT CONDITIONS

The ambient atmosphere at the intake end and the exhaust end are created by dragging the ambient icon from the model tree on to the canvas. The properties of the ambient air conditions are given in the properties window, as shown in Figure 4, with the atmosphere temperature set to 300 K and pressure set to 1 bar. For initial conditions, 100% fresh air is set. The diameter is set to 'AUTO', which sets the diameter same as the duct connecting to it with no restriction. The discharge coefficients, when set to 'AUTO' are automatically calculated by the software based on the Equation (4) as shown below.

$$C_D = 1 - \left[1 - \left[\frac{D}{D_1} \right]^4 \right] * \left[0.2 + 0.2 \left[1 - \left[\frac{D}{D_2} \right]^4 \right] \right] \quad (4)$$

where, D = Orifice diameter

D_1 = Upstream diameter

D_2 = Downstream diameter

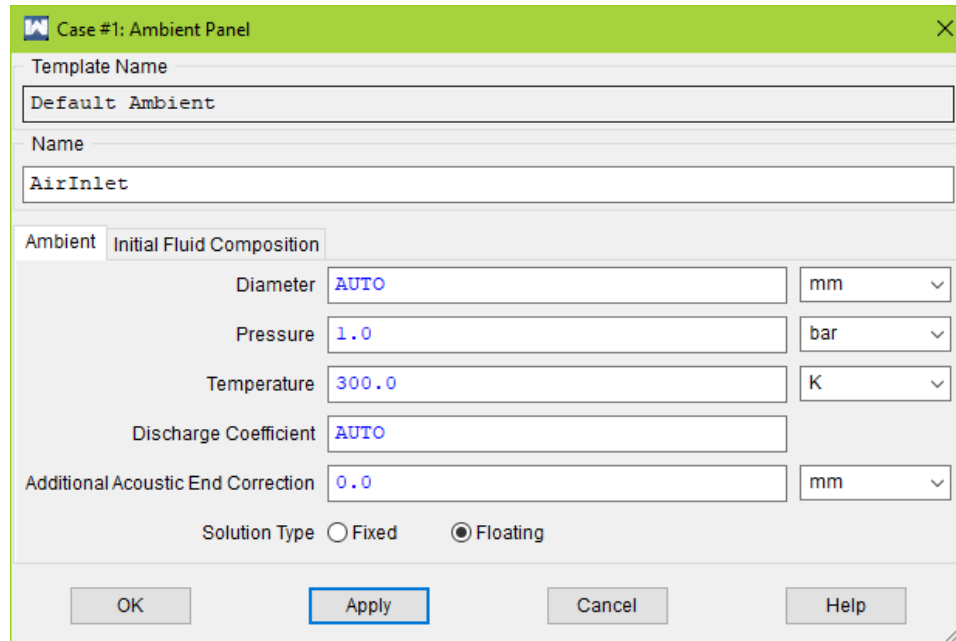


FIGURE 4: Air inlet ambient atmosphere properties window

2.1.3. CREATING JUNCTIONS

In a similar way, orifices are created by dragging the orifice icon on to the canvas. Orifice denotes the joints or junction between two parts. Alternatively, if the parts are connected by valves, valves can be used. The intake system of the engine is comprised of a throttle body, a 20 mm restrictor as set by the Formula SAE regulation, diffuser, plenum and runners which are finally connected to the intake port on the engine. The ducts represent the tubes, diffuser and runners. The ducts are created by dragging the pink dots to the next part – either the orifice, Y-junction, ambient, etc. When the duct is first created the ducts are highlighted in yellow indicating that some geometric data is missing. By default, when the ducts are first created, they have a diameter of value zero.

The orifices in-between such ducts convert to a dot as the ducts on either side have zero diameter.

2.1.4. DUCTS AND DISCRETIZATION

The duct dimensions are entered based on the left and right attachments. Figure 5 shows the diffuser connecting from the 20 mm restrictor to the plenum. Therefore its left diameter is 20 mm and right diameter is 42.86 mm as per the design. The overall length for this duct is 150 mm with a discretization length of 35 mm. The discretization length defines the length of each element. For higher resolution a smaller discretization length is required but slows down the simulation. The higher the elements, it is easier to model a travelling pressure wave [34]. Therefore, it is a compromise between accuracy and speed of simulation that defines the discretization length required. Figure 6 shows the relation of discretization length and the results. The wall friction and heat transfer coefficients are used as tuning coefficients, when actual data is not available, which represent the roughness of the material and flow conditions in the duct. The discharge coefficients are set to 'AUTO' and therefore calculated by the software based on Equation (4). All ducts are defined based on the dimensions and operating conditions in a similar way.

2.1.5. Y-JUNCTIONS

The plenum is created as a Y-junction with a volume of 3 liters as per the design. Y-junctions are used where volume has to be modelled that generally has more than one connection point. They are also used for representing arbitrary shapes with an aspect ratio inappropriate for modelling a duct. Y-junction is defined by a volume and surface area. A proportional type of fuel injector is added to the runner. Similar to the intake system, the exhaust system is defined. Similar to the intake system, the exhaust system is modelled with ducts and a Y-junction. The exhaust valves are connected to exhaust ports represented by ducts. These ducts connect to a Y-junction, which in turn connects to the exhaust runner.

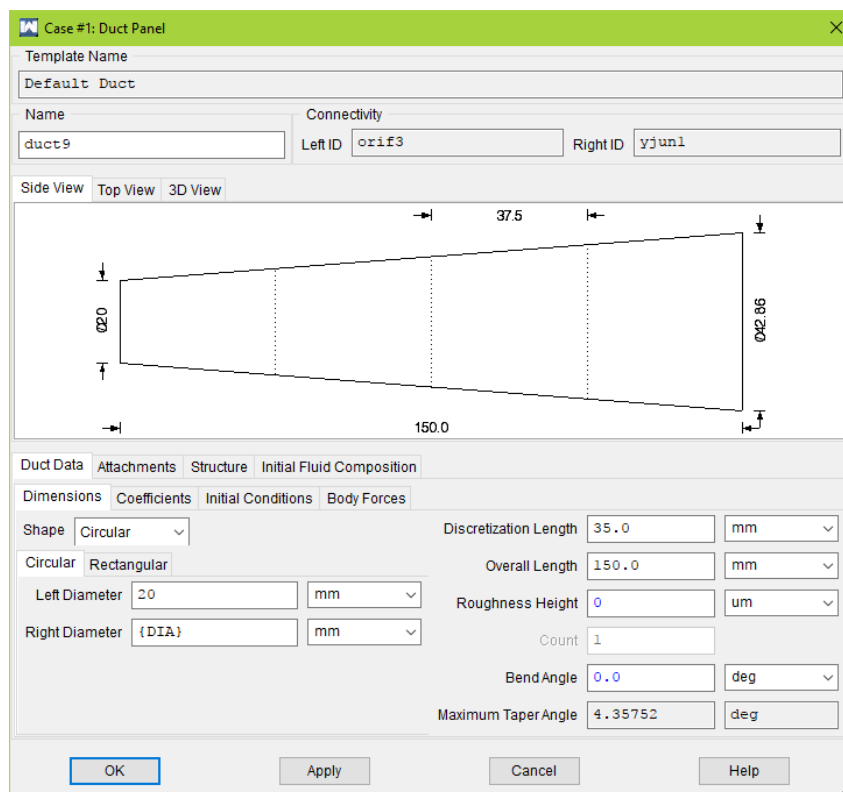


FIGURE 5: Dimension window for diffuser connecting restrictor to plenum

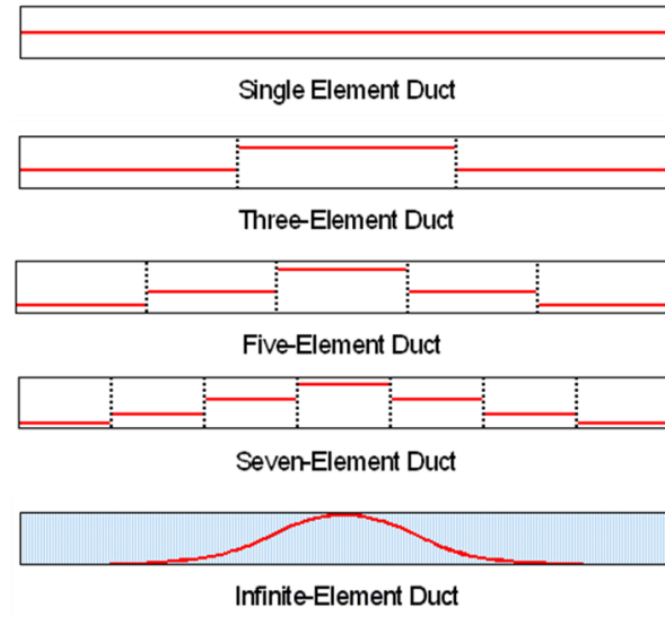


FIGURE 6: Relation between discretization and results [34]

2.1.6. DUCT INITIAL CONDITIONS

The exhaust runner is connected to the open atmosphere. The exhaust runner length is defined as a constant so that the runner length variation as proposed can be varied with different cases and checked for. A higher resolution discretization is given for the exhaust runner with a discretization length of 10 mm. As the research is focused on exhaust system, the higher resolution yields more accurate results. The exhaust runner editor window is shown in Figure 7. The initial conditions for the exhaust runner are set to 1.05 bar with gas temperature of 900 K and wall temperature of 700 K, shown in Figure 8. These values serve as a starting point for the software to calculate and reiterate the values in the following simulation cycles. In the engine simulation the gases move quickly and the values are re-calculated frequently [34].

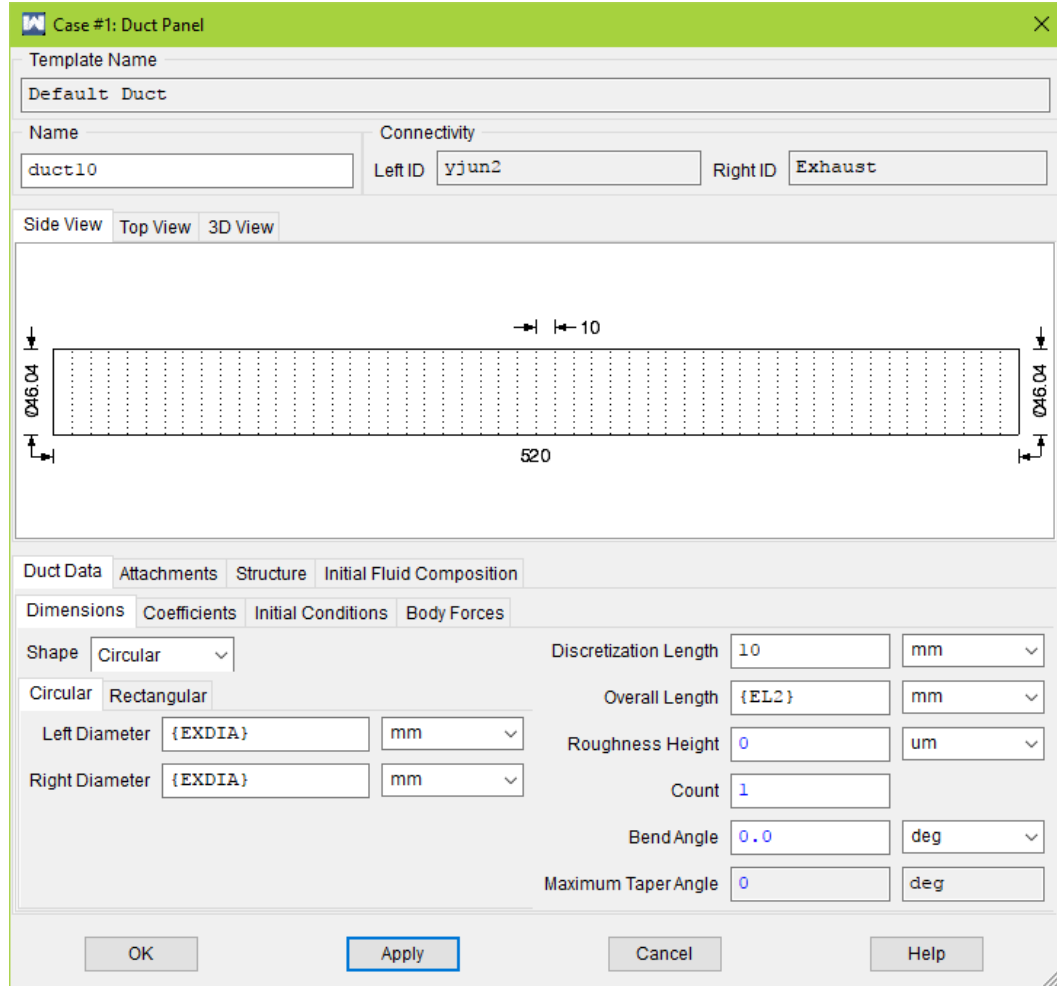


FIGURE 7: Exhaust runner editor window

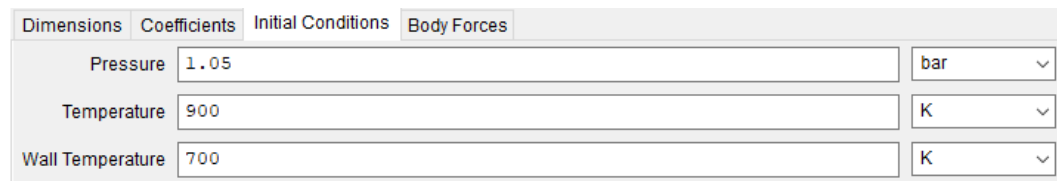


FIGURE 8: Initial conditions set for exhaust runner

2.1.7. BUTTERFLY VALVE

When all the ducts are defined the orifices shows up again, instead of dots. However, based on the diameters on left and right hand side, the illustrations are different for different cases. The different illustrations are shown in Figure 9 and are a good indication for the designer. The throttle body is created as a butterfly valve from the model option. The minimum/idle position is given as 5 degrees with the maximum automatically set to approximately 87 degrees by the software based on the bore diameter of 42 mm and shaft diameter of 2 mm. The throttle valve editor window is shown in Figure 10.

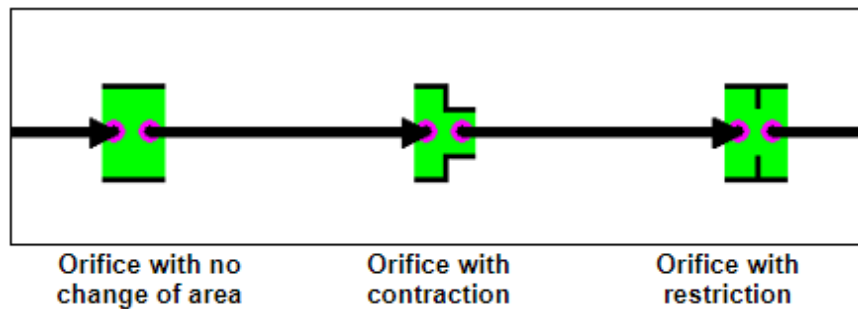


FIGURE 9: Dynamic display of the orifice element on canvas [34]

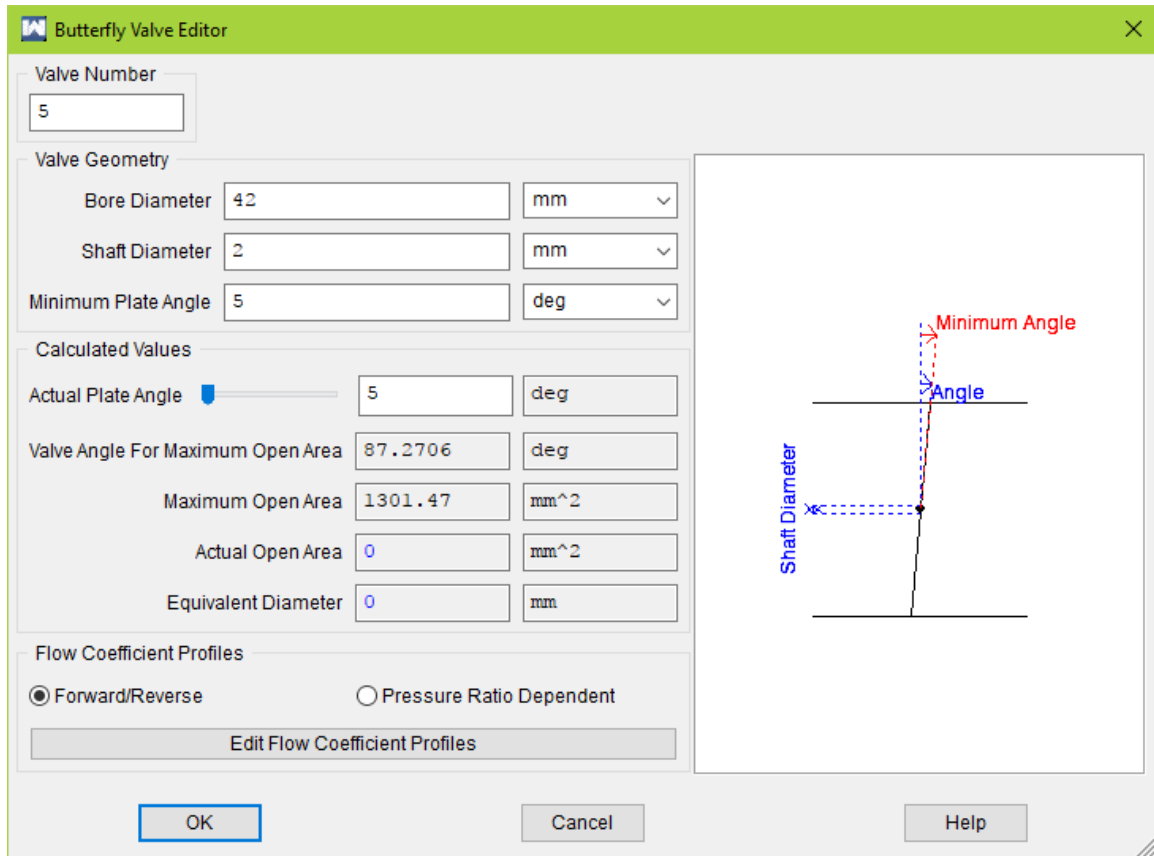
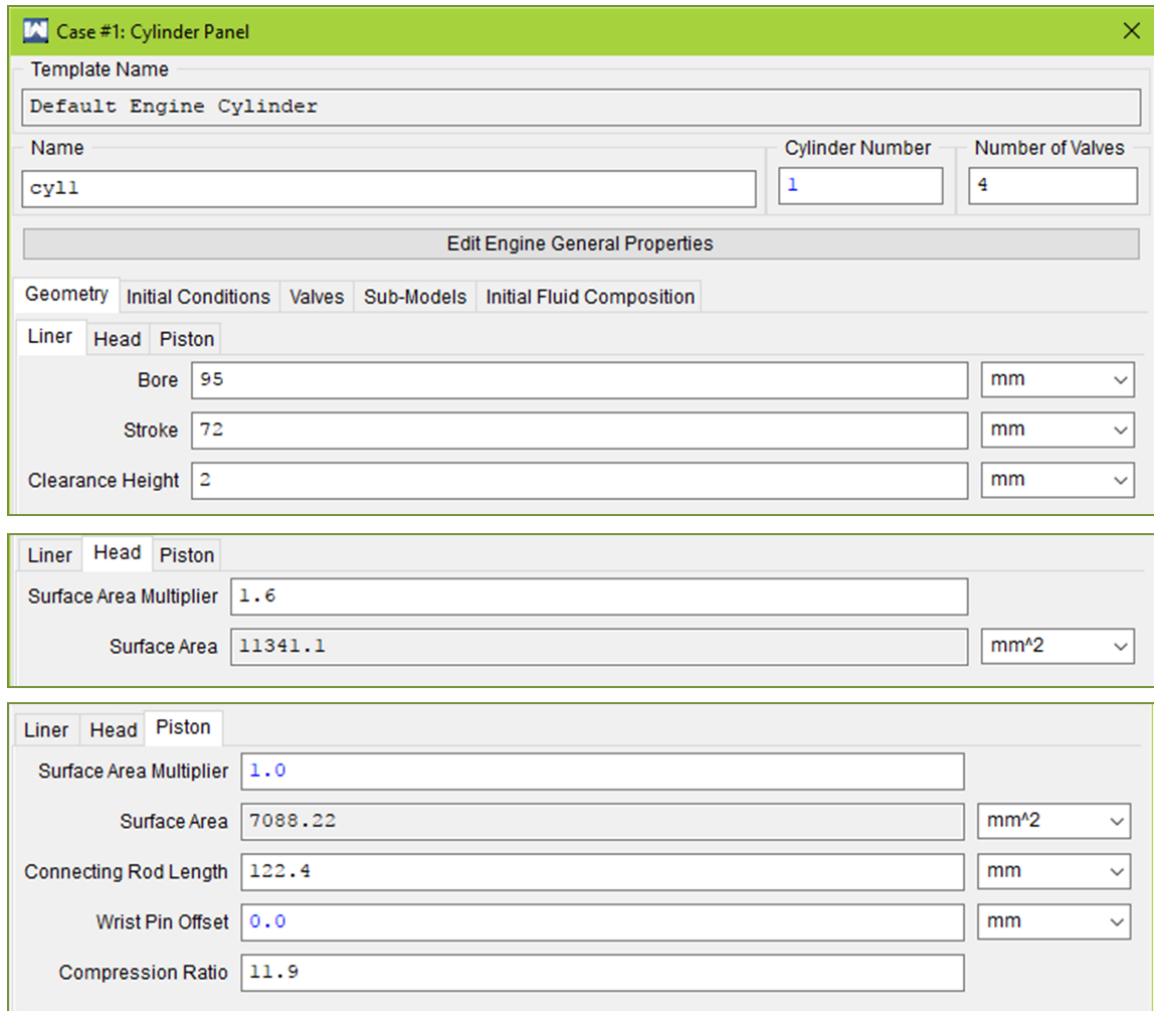


FIGURE 10: Throttle valve editor window

2.1.8. ENGINE SETUP

For defining the engine cylinder, the values of bore, stroke, clearance height and other dimensions are entered as appropriate from Table 1, which is shown in Figure 11. Apart from the dimensions, the engine has to be defined based on several other parameters. The number of cylinders in the engine, number of strokes and type of ignition system are to be entered in the window. Chen-Flynn friction correlation model was used for calculating FMEP (Friction Mean Effective Pressure). The equation used by the

software is given by equation (5) and the recommended values for these terms are shown in Table 2. The engine general panel window is shown in Figure 12.



Case #1: Cylinder Panel

Template Name: Default Engine Cylinder

Name: cyll Cylinder Number: 1 Number of Valves: 4

Edit Engine General Properties

Geometry Initial Conditions Valves Sub-Models Initial Fluid Composition

Liner Head Piston

Bore: 95 mm

Stroke: 72 mm

Clearance Height: 2 mm

Liner Head Piston

Surface Area Multiplier: 1.6

Surface Area: 11341.1 mm²

Liner Head Piston

Surface Area Multiplier: 1.0

Surface Area: 7088.22 mm²

Connecting Rod Length: 122.4 mm

Wrist Pin Offset: 0.0 mm

Compression Ratio: 11.9

FIGURE 11: Engine cylinder dimension window

$$FMEP = ACF + BCF(P_{\max}) + CCF \left(RPM * \frac{stroke}{2} \right) + QCF \left(RPM * \frac{stroke}{2} \right)^2 \quad (5)$$

where, ACF = constant portion of the Chen-Flynn friction correlation

P_{\max} = peak cylinder pressure

BCF = account changes in P_{\max} , varies linearly with peak cylinder pressure

CCF = term which varies linearly with the piston speed, accounts for
hydrodynamic friction in the power cylinder

QCF = term which varies quadratically with the piston speed, accounts for
windage losses in the power cylinder

stroke = cylinder stroke

TABLE 2: recommended values for Chen-Flynn friction correlation equation

Friction correlation coefficient	Value
ACF	0.35 bar
BCF	0.005
CCF	400 Pa/min*m
QCF	0.2 Pa/min ² *m ²

Case #1: Engine General Panel

Geometry | **Operating Parameters** | Scavenge | Combustion | Conduction | Heat Transfer | Turbulence and Flow | Head Geometry | Slaved Models

Configuration

No. of Cylinders: 1

Strokes per Cycle: 4

Engine Type: Spark Ignition

Displacement: 0.510352 1

Imposed Piston Motion

Printout Flag

In-Cylinder State: 0

Port Conditions: 0

Friction Correlation

ACF: 0.35 bar

BCF: 0.005

CCF: 400 Pa*min/m

QCF: 0.2 Pa*min²/m²

Firing Order and Relative TDC

	1
Cylinder	1
TDC	0.0

Required for Swirl Prediction

Piston Bowl Depth: 0.0 mm

Piston Bowl Diameter: 0.0 mm

Piston Bowl Rim Diameter: 0.0 mm

Piston Bowl Volume: 0.0 mm³

OK Apply Cancel Help

FIGURE 12: Engine general panel window

2.1.9. CONSTANTS

In the operating conditions, the engine speed is entered as a text string. These strings are called ‘Constants’ in Wave and help in defining multiple cases for comparing and also for obtaining continuous data. Entering engine speed as a constant will enable obtaining data for the complete engine speed range of 1000 RPM to 11000 RPM. For variation of runner length, valve timing and lift as well, the ‘constants’ will be used.

2.1.10. COMBUSTION MODEL

For spark ignition type engine, four combustion sub-models are available - the Profile, SI Wiebe, Multi-Component Wiebe, and SI Turbulent Flame sub-models. If the fuel mass burn versus CA data is available for every speed and load point, Profile sub-model can be used. Multiple-Component Wiebe sub-model is generally used for non-conventional combustion systems by overlaying multiple burn patterns to form a complex burn profile. SI Turbulent sub-model is a complex predictive combustion sub-model which is used in advanced simulations. SI Wiebe sub-model is most widely used, which uses an S-curve function representing the fuel mass burn fraction with respect to time. The first derivative of this function is the mass burn rate. This sub-model is commonly used and represents experimental data well [34].

2.1.11. HEAT TRANSFER MODEL

The combustion model window is shown in Figure 13. For convective heat transfer, Woschni Correlation is the most commonly used sub-model. The sub-model assumes heat transfer of a confined volume through all the surrounding walls, in this case, the piston face, cylinder walls, head, valves, etc. The area of these components is calculated by the dimensions and ratios given when defined the parts.

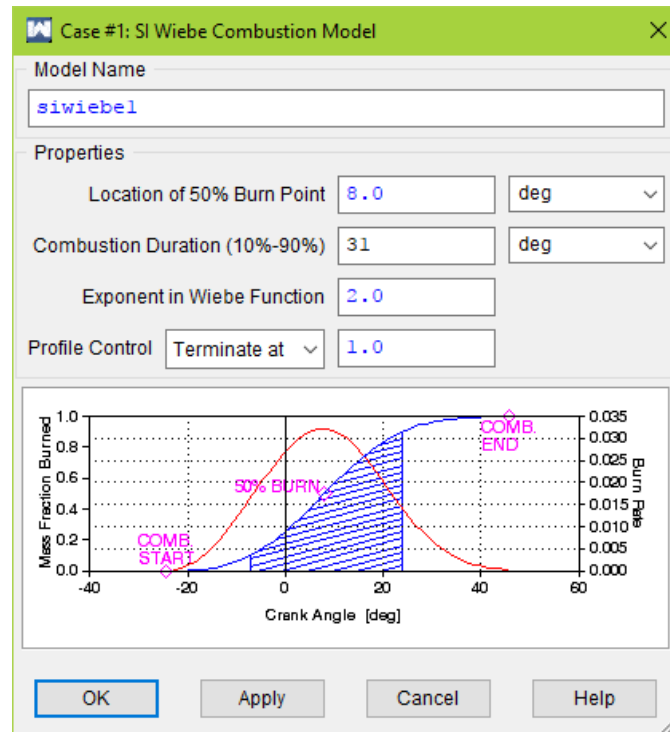


FIGURE 13: Combustion sub-model window

2.1.12. POPPET VALVES

Intake and exhaust valves are defined as global valves, that is, an intake/exhaust valve modelled can be used at all the locations and for all cylinders using the single global valve modelled. Lift type valve is created for a poppet valve, which is the most common type. The intake valve diameter as measured is entered. The lift profile as measured by a dial gauge against CA is entered in the lift profile table. Similarly, the valve profile is modelled for the exhaust valve. The exhaust valve profile as created in the software is shown in Figure 14. The valve timing and lift multiplier as set as constants so that they can be varied between different cases. The complete 1-D model is shown in

Figure 15. As described, the model comprises of open atmosphere for fresh air, throttle body, 20 mm restrictor connected to a 3 liter plenum via a diffuser, intake runner, single combustion chamber with 4 valves and exhaust runner.

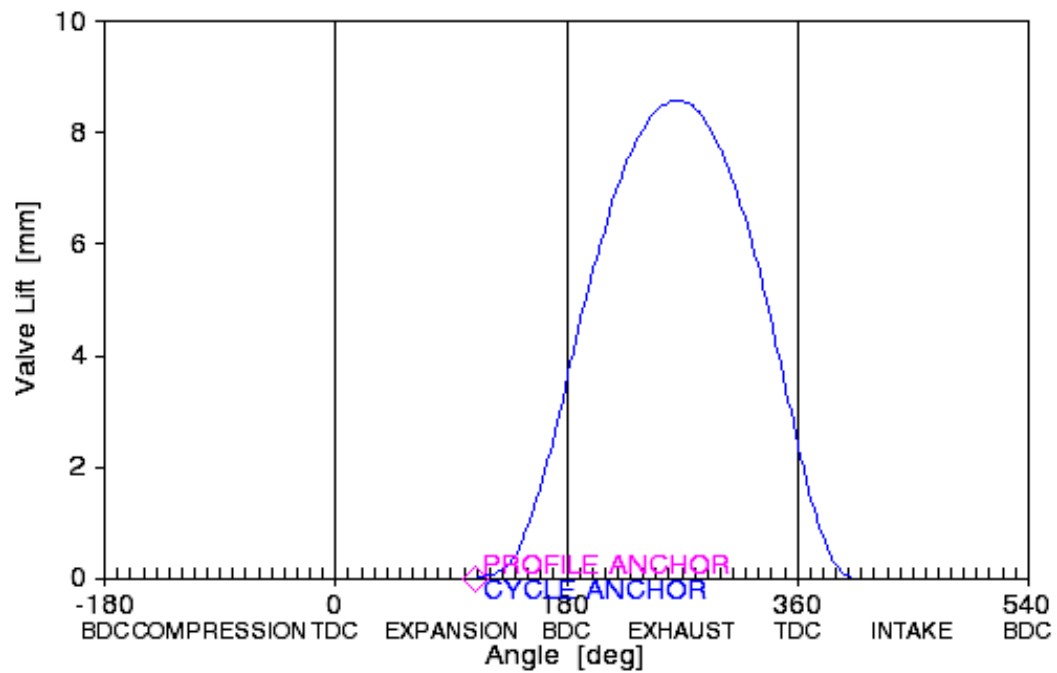


FIGURE 14: Exhaust valve profile as shown in Ricardo Wave based on user input

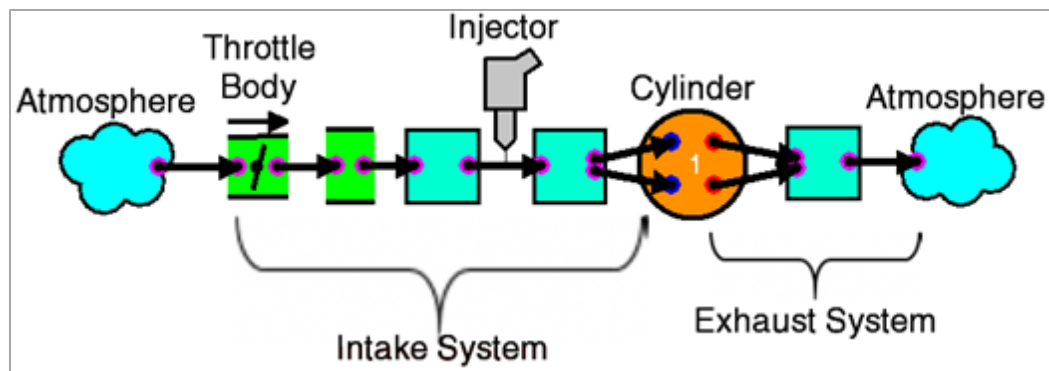


FIGURE 15: 1-D model as prepared in Ricardo Wave

2.2. VALIDATION OF THE MODEL

Based on the one-D model prepared, the power and torque curves are compared with the data available from the chassis dynamometer. In the post-processing window, WavePost, the generated output of power and torque curves are overlaid by the data available from the chassis dynamometer. WavePost has an option to import data from excel or data from ASCII (American Standard Code for Information Interchange) file. The comparison of the two outputs is shown in Figure 16. The data obtained from the chassis dynamometer includes frictional and transmission losses incurred by the gearbox, drive shafts and the wheel and hub parts and thus are lower than that at the engine. Therefore, the curves are offset to that seen in the software. However, it can be observed that the trend of the curves throughout the engine RPM range remains the same. The divergence between the chassis dynamometer data and the software data is mainly at higher engine speed. This could be due to the increased frictional losses at the transmission and wheels. The engine torque curve for the chassis dynamometer data starts rising from 5000 RPM as the clutch was disengaged at this engine speed when the dynamometer test was performed. Therefore, any improvements seen with the help of this software will yield similar results in the physical setup. The effects of these changes can be thus studied without any physical tests before arriving at a more optimal design.

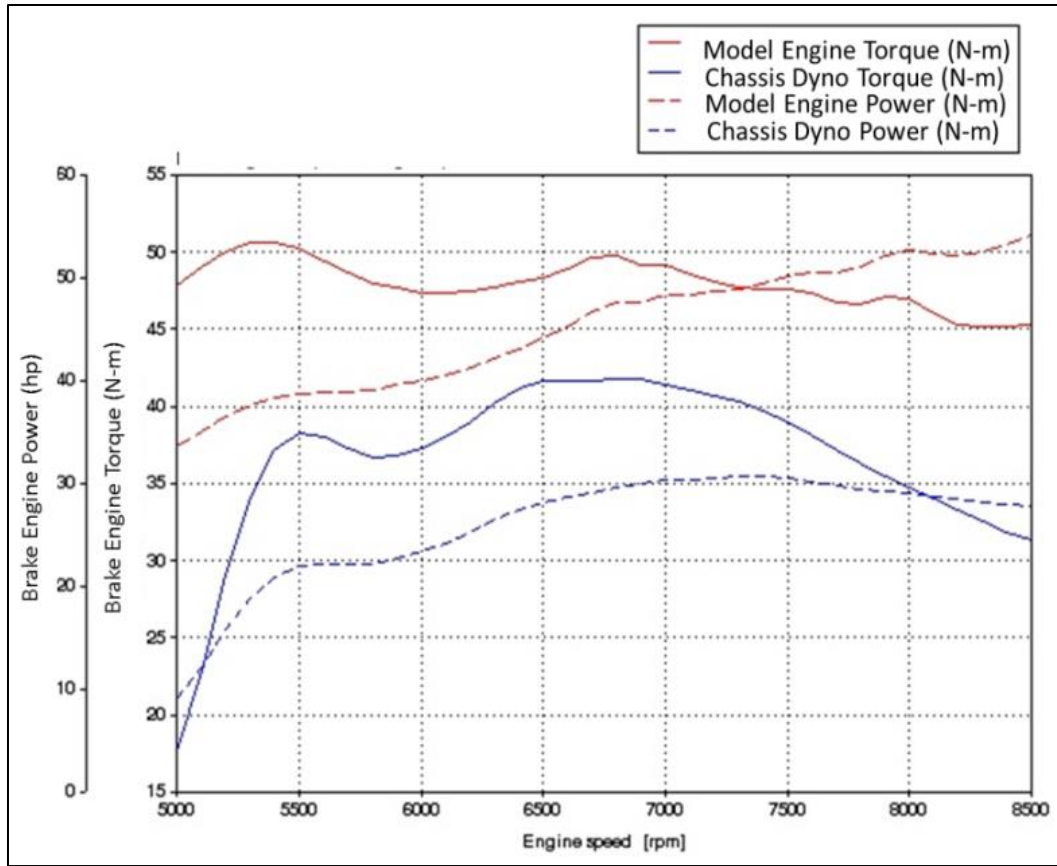


FIGURE 16: Engine Torque (N-m) and Engine Power (hp) comparison between simulation and chassis dynamometer

2.3. CASE SETUP

The software allows to check if all the entered inputs are acceptable for the solver to process. Though WaveBuild has many error checking mechanisms, the solver will check if all settings are good and if the solver will run. When the Run Input Check icon on the toolbar is clicked, the solver will run an input check for all elements in a shell window and displays the progress. An output file is generated and if any errors are noted, they can be checked in detail from the output file. Time plots can be added to any part, like intake runner, exhaust port, etc. These time plots are created if the user needs some pressure, velocity or mass flow data at a particular location. In this case, to monitor the pressure waves in the exhaust system, a time plot for pressure is created close to the exhaust valve. The duct representing the exhaust port is instrumented with a pressure sensor in WaveBuild at a distance of approximately 9 mm from the exhaust valve. The time plot window for the pressure sensor is shown in Figure 17. In addition to this, a pressure sensor is also placed in the intake port and mass flow sensors are placed at the intake and exhaust valves. Location of sensors depends on the number of discretization elements for that duct. Similarly, if desired, time plots can be created for combustion cylinder to obtain P-V diagram (Pressure Volume curve), piston velocities, etc. Multiple plots can be overlaid as well if similar data curves are contained in the plots. When the simulation is completed, .OUT file is generated which consists of all the output information in a text file format. Results can be studied from this text file, but use of Ricardo software's post-processing tool, WavePost, gives a better illustrative perspective.

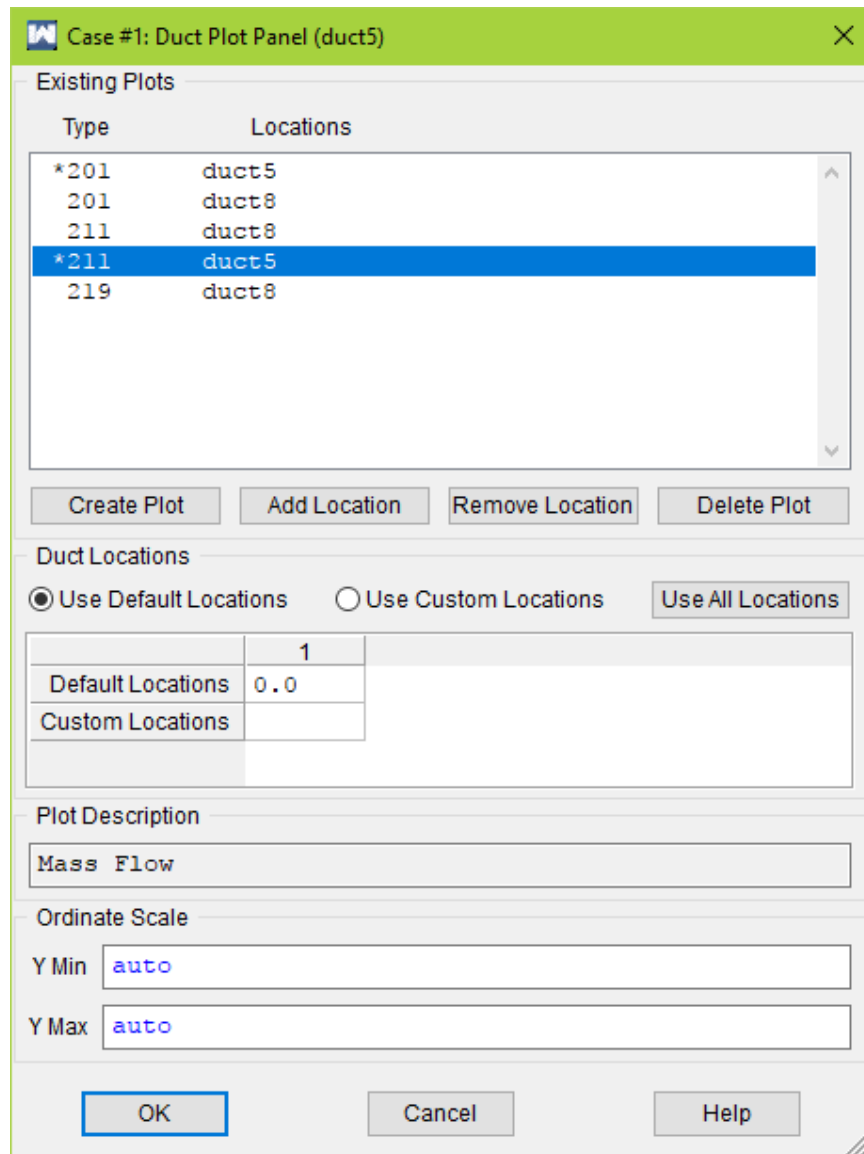


FIGURE 17: Time plot editor window for pressure sensor in exhaust port

The analysis took place in two major steps. Initially the exhaust runner length is changed and then combined with the exhaust valve opening time. This study captured a number of effects that were affected by the runner length on the performance of the engine. With the tuned runner length, the exhaust valve timing was studied and tuned. With the combined effect, several observations were made and the findings were presented at the ASME 2017 International Mechanical Engineering Congress & Exposition in Tampa, FL [37]. With the use of variable case setup option, parameters defined as ‘constants’ in WaveBuild can be varied. The total runner length of 520 mm was split into 3 segments and the middle segment was used as a variable length segment. The length of this segment was varied from 100 mm to 2000 mm in increments of 20 mm. The valve timing was varied from 80° aTDC to 120° aTDC in increments of 1° keeping the tuned runner length sequence unchanged. Based on the results obtained, the case setup was decided for further study.

The valve lift was varied in combination to the runner length and valve timing for second stage of analysis. In this study, the combined effect was studied with all variables changed simultaneously to understand the interrelated behavior of these parameters. The exhaust runner length is varied from 40 mm to 1000 mm in steps of 40 mm with the original runner length being 520 mm. The exhaust valve opening is varied from 84° aTDC to 110° aTDC in steps of 2° and 108° aTDC being the actual valve opening time. The actual exhaust valve lift is 8.6 mm. The lift is varied from 0.8X to 1.2X (6.9 mm to 10.3 mm) of the original lift in steps of 0.1X (0.86 mm). The valve open duration is kept constant. The variation of runner length, valve timing and lift for this stage is shown in Figure 18.

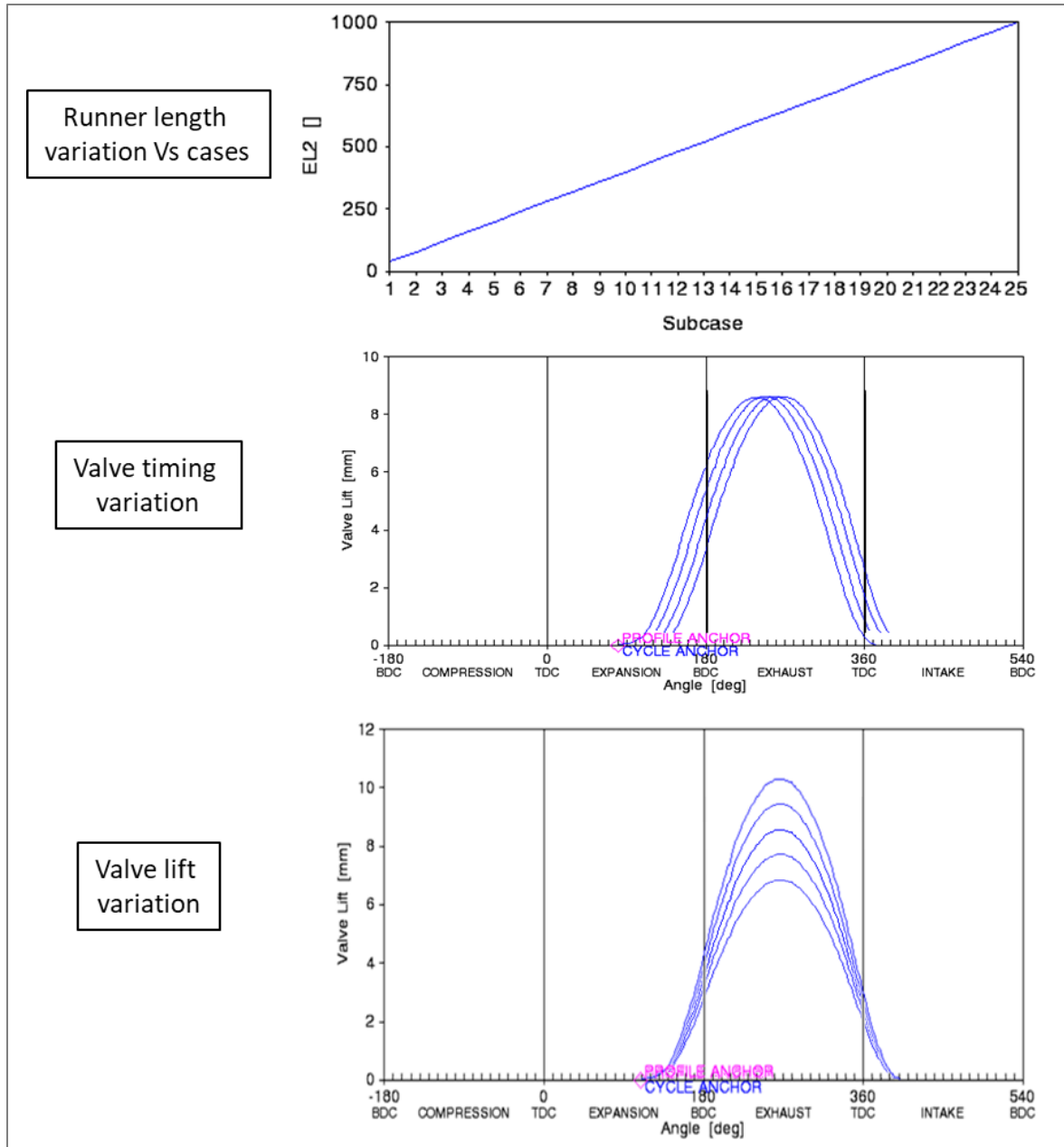


FIGURE 18: Case setup for runner length, valve timing and lift variations in exhaust system

CHAPTER 3: RESULTS AND DISCUSSIONS

3.1. INITIAL STUDY WITH RUNNER LENGTH AND VALVE TIMING

For the first case setup discussed, the effect of exhaust runner length and exhaust valve timing was studied. The runner length was varied and based on the results, the length was optimized. Post which the runner length was fixed at the optimum setup and the valve timing was varied and the effects are studied.

3.1.1. EXHAUST RUNNER LENGTH

For the first set of analysis, the engine torque achieved was observed for each length along the complete engine speed range. Figure 19 shows the absolute engine torque achieved against length and engine speed. The overall peak torque of 50 Nm was achieved at 6500 RPM for the length 540 mm. If the peak engine torque achieved at 3000 RPM is checked, for a length as long as 1800 mm, 45 Nm is achieved. Contrast to this, at 11000 RPM the peak torque of 30 Nm is achieved at a short length, 120 mm. Figure 19 does not give a perspective view of the engine behavior with respect to the length although it shows the absolute values. From literature review, it is understood that the length is a function of the engine speed. It was seen that at high engine speeds the local peak torque value was achieved at a shorter length as compared to lower engine speeds where the length was very long.

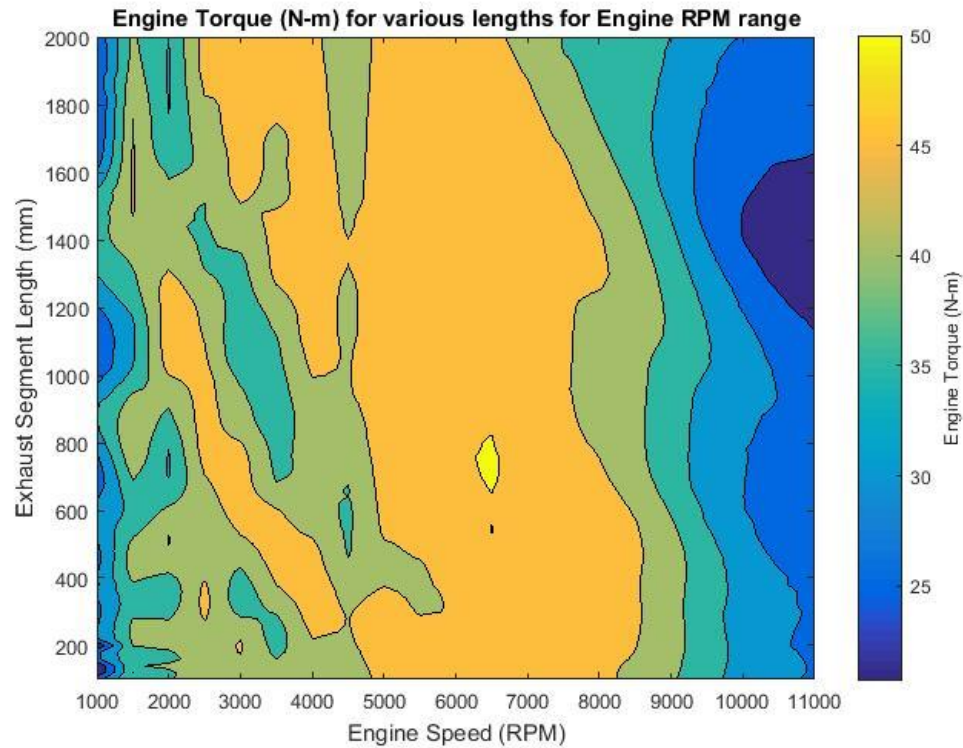


FIGURE 19: Torque values at different engine speeds for different lengths

If for each engine speed, the peak torque at that engine speed is used as the maximum possible engine torque that can be achieved for that engine speed, the deficiency with using other lengths can be observed. For example, if the maximum torque achievable at 3500 RPM is 47 Nm with 460 mm segment length, the deficiency at this point is zero, but for the same engine speed, for a 220 mm segment length, the torque than can be achieved is approximately 38 Nm, therefore at this length deficiency of 9 Nm is present. Figure 20 gives the deficiency plot for all engine speeds for the lengths analyzed for. The dark regions represent low deficiency zones and the lighter colors represent high deficiency zones. Low deficiency indicates high engine torque and

therefore it was ideal to stay in these zones. Similarly high deficiency denotes low performance and it was ideal to stay out of this zone. It can be observed that for any single runner length only a certain engine speed range performs well. It can be noted that the lengths seen for peak engine torques at 3000, 6500 and 11000 RPM fall in the dark region. The dark region is connecting all these points.

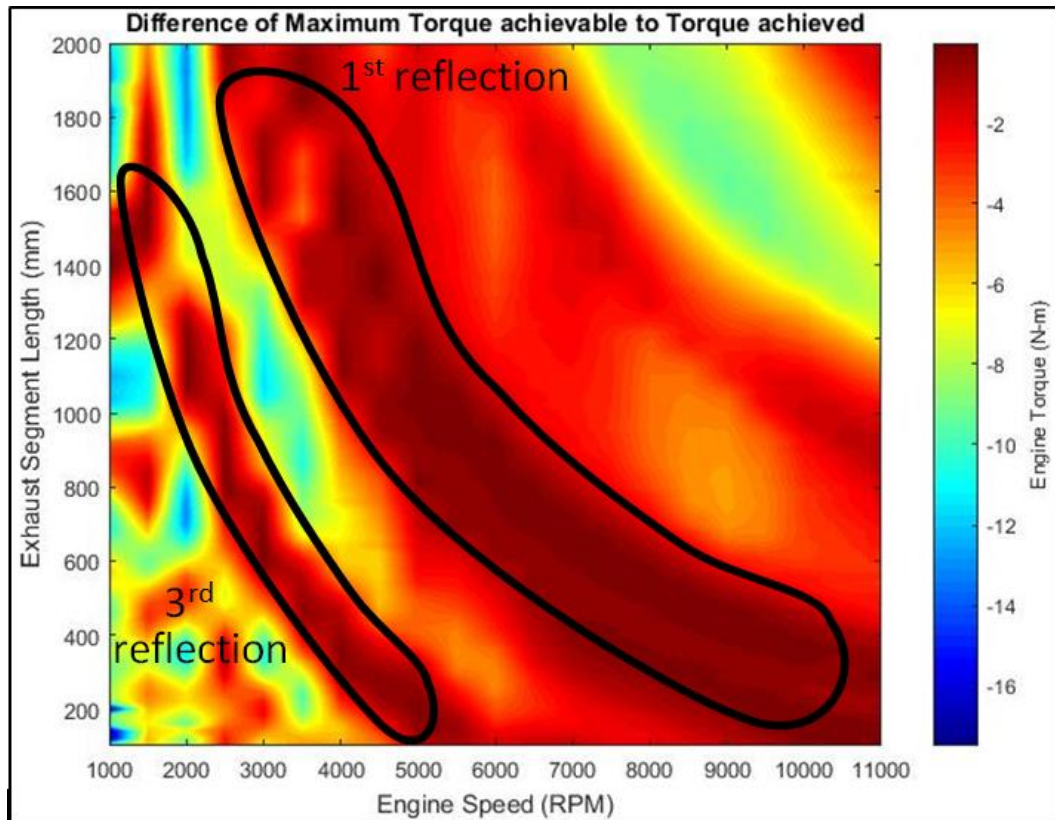


FIGURE 20: Engine torque deficiency plot for all engine speeds for all the lengths analyzed

The 1st reflection zone highlighted in figure 20 represents the engine torque achieved for the first rarefaction wave reflected from the end of the runner. The curve

formed by the dark region represents an exponential curve demanding more length at lower engine speeds. Since the lengths cannot be packaged beyond a certain limit, the exponential requirement cannot be catered for. Figure 20 shows a similar curve marked as 3rd reflection. If the exhaust valve remains closed, when the first rarefaction wave returns, the wave reflects against the closed valve. The following reflection is a compression wave and the 3rd reflection is a rarefaction wave. Though for every reflection the engine torque decreases, it is a compromise between length and performance. If the exhaust valve opens for the 2nd reflection, which is for the compression wave, the pressure differential between combustion chamber and exhaust port drops and the scavenging efficiency is lowered. Therefore, the performance was low and this region was to be avoided.

Figure 21 shows the engine torque for lengths up to 600 mm for 3500 RPM. The peak engine torque was achieved for the rarefaction wave and low value for the compression wave. For a length of 220 mm the engine torque was of the least value at about 38 Nm and for a length of 460 mm the torque value was the highest, which was about 47 Nm. Figure 22 shows the pressure traces near the exhaust valve in the exhaust port and the mass flow at the intake valve. Point marked 1 represents a rarefaction wave at EVO and point marked 3 represents a compression wave at EVO. Point 1 was for 460 mm length for which peak engine torque was observed in Figure 21. Whereas, point marked 3 was for a length of 220 mm, where the lowest engine torque was seen.

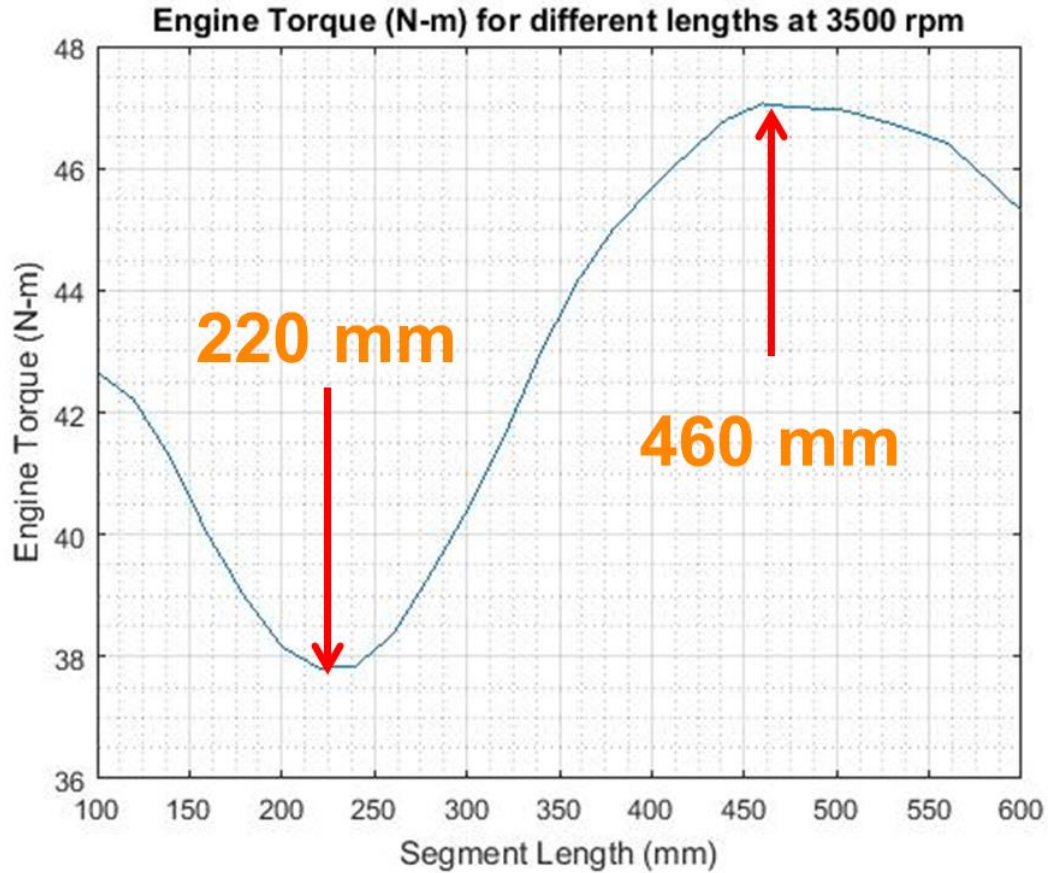


FIGURE 21: Engine torque for different lengths for 3500 RPM

As the rarefaction returns when exhaust valve opens for 460 mm length, the pressure differential is much higher and therefore the exhaust gases flow out with high force. The pressure rise for 460 mm after exhaust valve opens was higher than that of 220 mm for the same reason. The corresponding intake flow for 460 mm length is given by point marked 2 and for length 220 mm is given by 4. It can be seen that the intake flow drops when intake valve opens at point 4. This is because the compression wave, that reflected, affects the intake flow by created a local high pressure zone obstructing the exhaust gas evacuation. Whereas for 460 mm length, as the intake valve was opened, the intake flow was established and a good cylinder filling was achieved. There by increased the volumetric efficiency and engine torque. Though the intake flow peaks for 220 mm

length, it can be observed that the area under the 460 mm length curve is more, indicating more intake mass flow during the intake stroke. Table 3 shows the volumetric efficiency, scavenging efficiency and residual fraction for the two lengths.

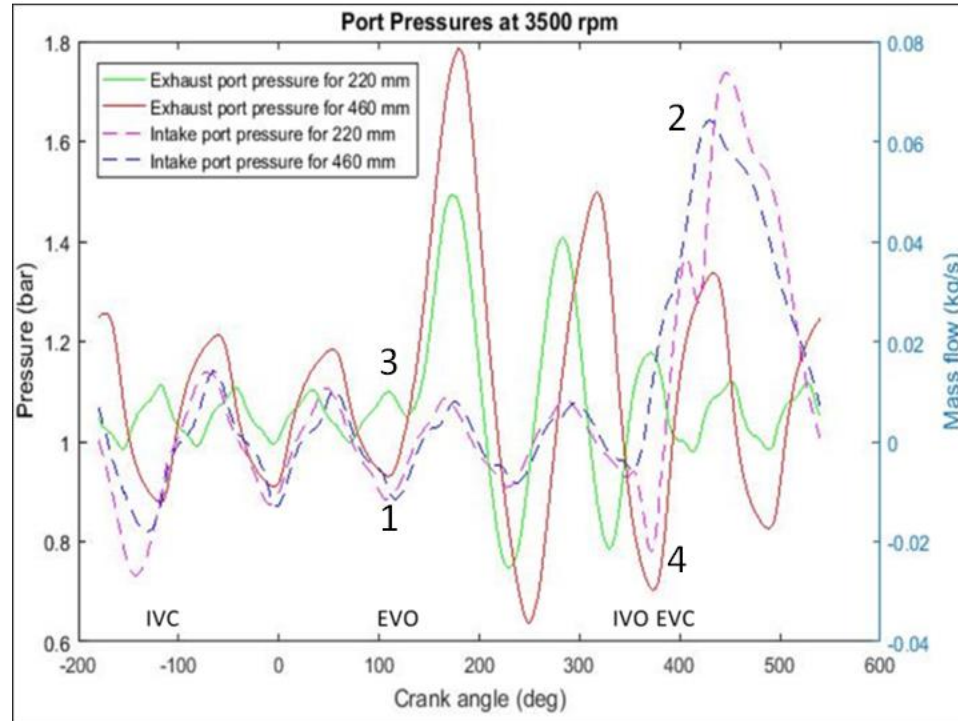


FIGURE 22: Pressures traces in exhaust port near exhaust valve and intake mass flow (kg/s) at intake valve for 3500 RPM

TABLE 3: Comparison of the performance for the two segment lengths

Segment length	Volumetric efficiency	Scavenging efficiency	Residual fraction
220 mm	0.741	0.921	7.882
460 mm	0.909	0.983	1.727

3.1.2. REFLECTIONS

The effect of the pressure waves decrease for every reflection. The compression waves see a drop in the high pressure value and rarefactions see an increase in low pressure values. As the pressure intensity drops for both compression and rarefaction waves, the effect of these waves also decrease for every reflection. The intensity is also referred to as the pulse strength. Figure 23 shows the engine torque achieved for 1500 RPM for all the runner lengths checked for. The peaks marked 1 to 5 drop as the length decreases. The peaks are in the order of the reflections. The peak engine torque values drop for every reflection. Therefore, it is ideal to use the earliest reflection to take benefit of the pulse strength.

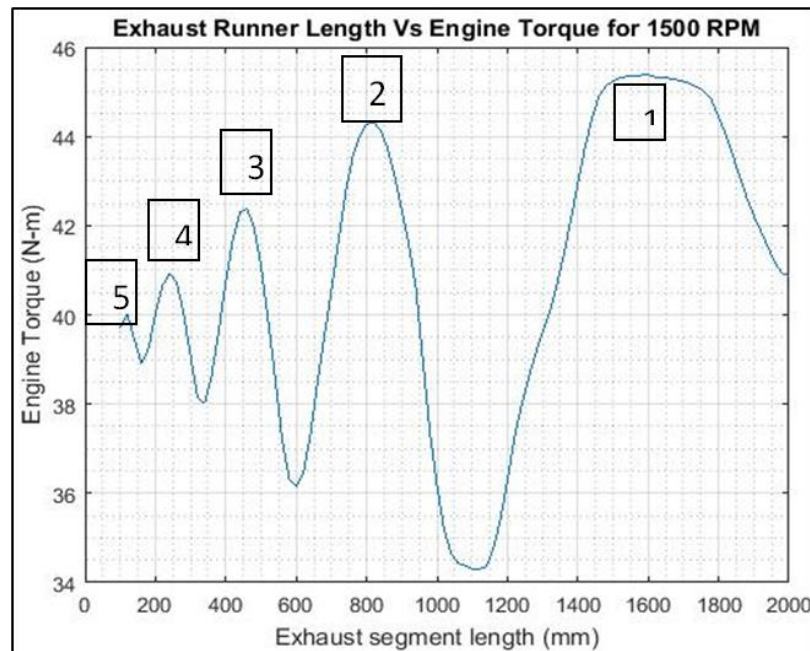


FIGURE 23: Engine torque at a 1500 RPM for different lengths

As the length of the exhaust runner length is limited by packaging constraints, the high runner length requirements at low engine speeds cannot be achieved. Therefore, to gain benefit from the rarefaction waves, later reflections have to be used. Assuming a continuously varying runner length system, the variation has to follow a sequence. For higher engine speeds, where the peak performance is expected, can take advantage of the first rarefaction reflection. However, lower engine speeds will have to use later reflections. As the runner length variation is to be in a sequence, the runner length had to shift from 1st reflection zone to the later reflection zones. Figure 24 shows a possible sequence, marked with white dashed line, for the recommendations made above. In the sequence shown, the length was limited to 600 mm. Therefore, the 1st reflection curve was used only from 11000 RPM to 6000 RPM. For lower engine speeds, the next reflection had to be used. As the sequence shifts from 1st reflection to the 3rd reflection, it passes through the 2nd reflection (lighter region) where the engine suffers in performance. This was due to the compression wave as mentioned earlier. For a continuous runner length change, this was unavoidable. The rate at which the shift takes place is also limited by the mechanical components.

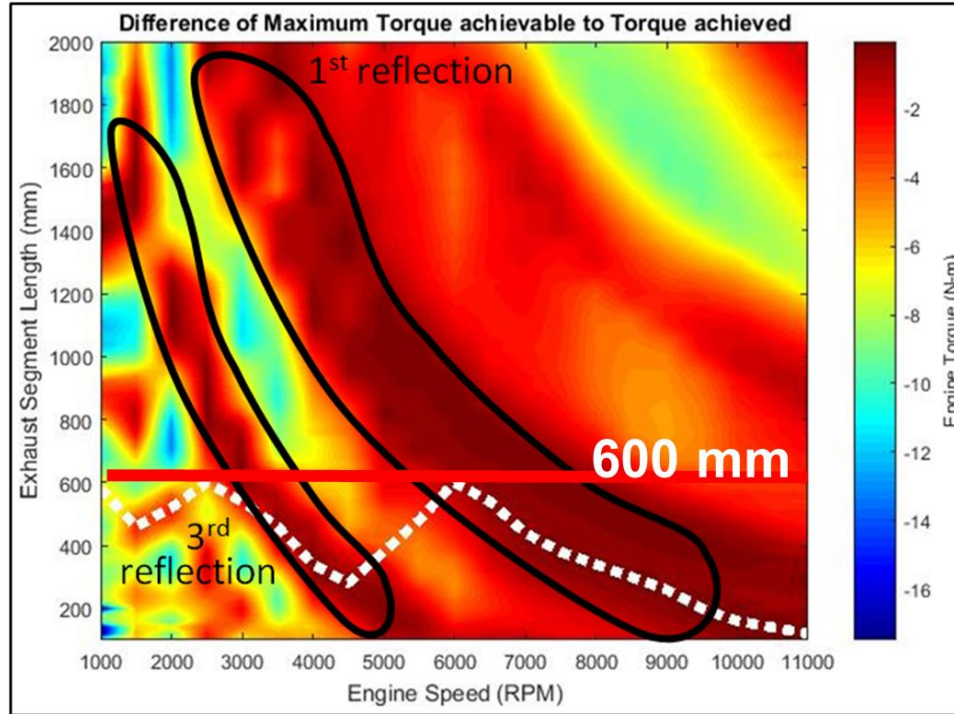


FIGURE 24: Sequence of lengths that can be chosen limiting it to 600 mm

3.1.3 EXHAUST VALVE TIMING

After the optimum length sequence was obtained, for this sequence, the valve timing was varied from 80° to 120° aTDC for all engine speeds, whilst keeping the valve open duration and lift constant. The effect of the variation of valve timing for 1000, 4500 and 7000 RPM are shown in figures 25 to 27. From the three figures, it can be observed that the engine torque reaches a peak value at some valve timing and then drops. The peak values are at different valve timings at different engine speeds. As the engine speed increases, the exhaust gases need more time to evacuate and hence demands for advancing the valve opening timing. Figure 28 shows the valve timing that is most suitable for this analysis. The dashed white line represents the valve timing versus engine

speed. At lower engine speeds, as seen from figure 24, the number of reflections is high and the effect of the wave is less significant below 3000 RPM. At engine speeds less than 3000 RPM, the valve timing was retarded as engine speed increased. This was because the power stroke was increased by opening the exhaust valve late and the effect of the high number of reflections is less effective.

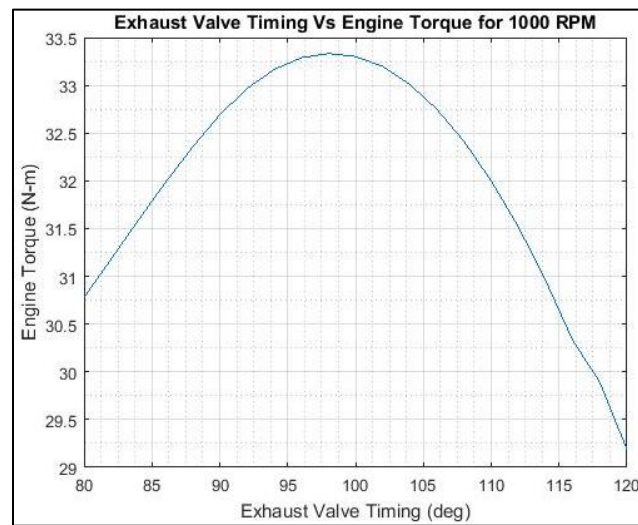


FIGURE 25: Engine torque at 1000 RPM for different valve timings

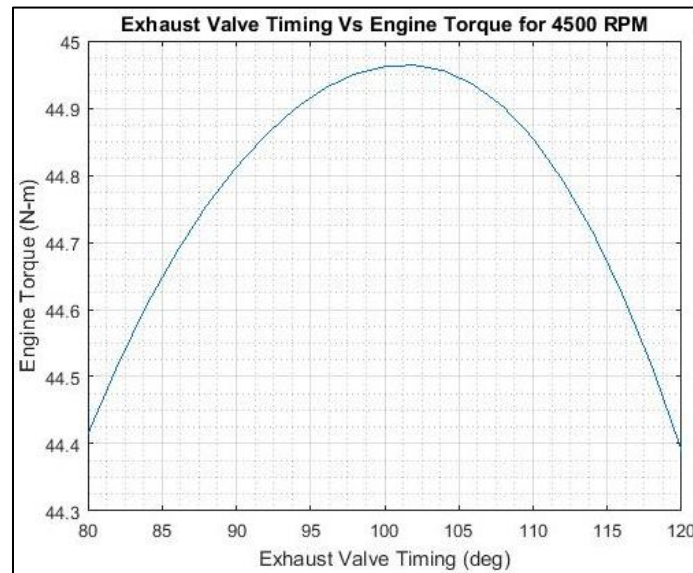


FIGURE 26: Engine torque at 4500 RPM for different valve timings

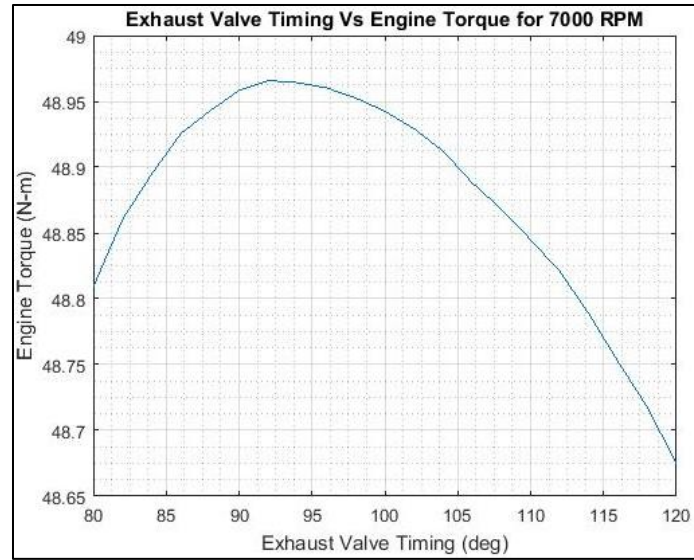


FIGURE 27: Engine torque at 7000 RPM for different valve timings

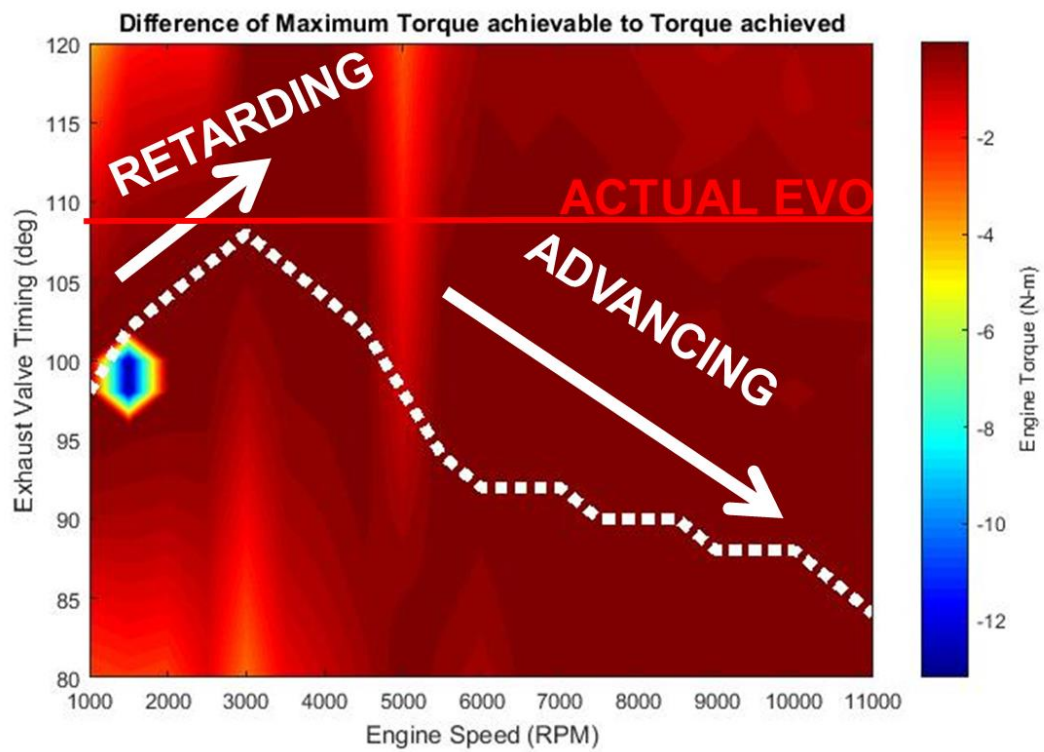


FIGURE 28: Sequence of valve timings that can be chosen

3.1.4. OBSERVATIONS

Based on the results above, the possible improvements in engine torque can be seen in figure 29 and 30. Figure 29 shows the maximum possible engine torque with variable runner length system and valve timing system alone and the combined improvement as well. Figure 30 shows the engine torque possible with length limited to 600 mm, valve timing and the combined effect of limited length and valve timing. With limited length, the performance of the engine was lowered at certain engine speeds. This cannot be avoided as there exists space limitations in vehicles. The percentage improvement for these two cases is shown in figures 31 and 32. From these two figures, it can be observed that the improvements are quite high at certain engine speeds, where the actual performance is very low. The improvements seen are in the range of 1 % to 2 % at low engine speeds and little to no improvements at high engine speeds with variable valve timing alone. With variable length, the improvements range from 4 % to 6 % and about 1 % at low and high engine speeds respectively. Whereas, the combined effect of variable length and valve timing shows improvements of 5 % to 8 % and 1 % to 2 % at lower and higher engine speeds respectively.

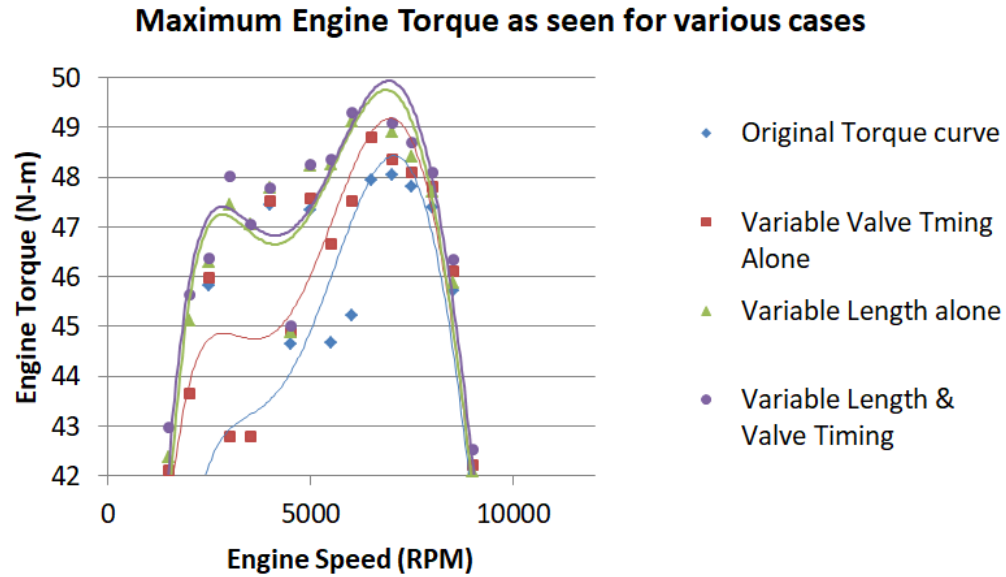


FIGURE 29: Improvement possible by having a totally variable length system

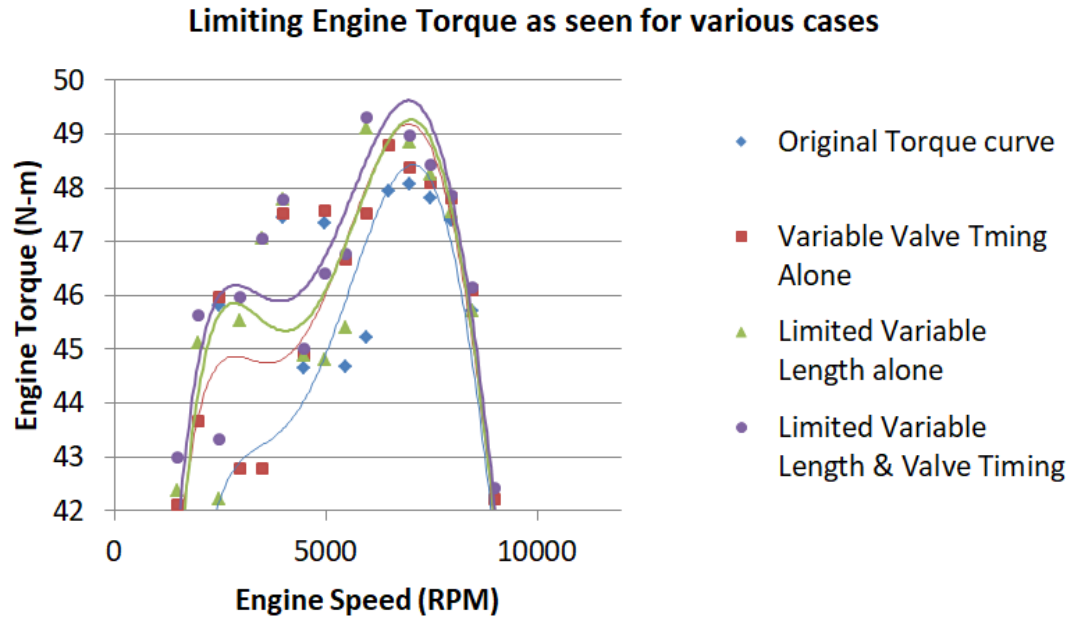


FIGURE 30: Improvement possible by having a limited variable length system

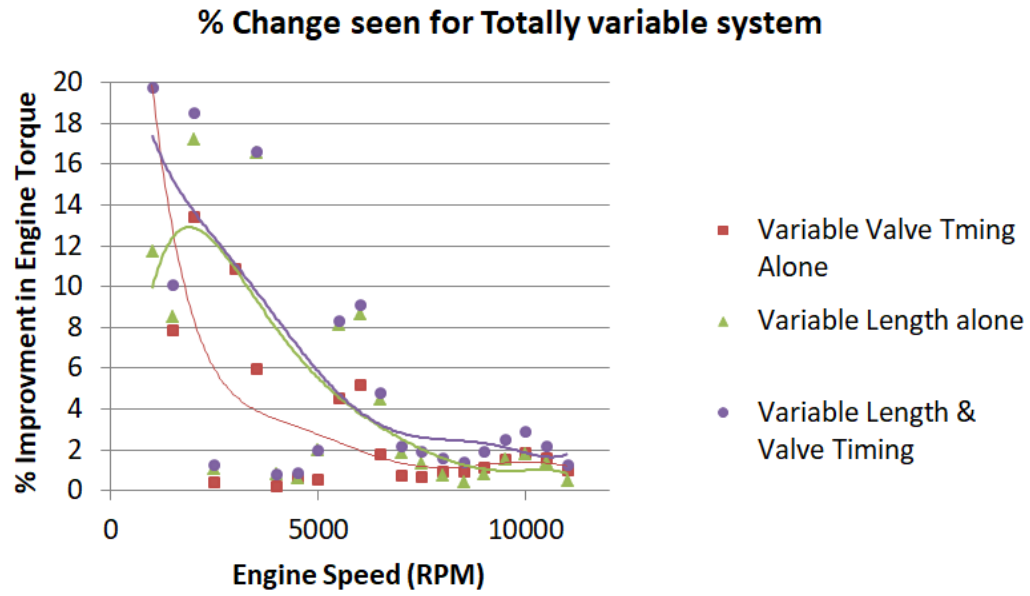


FIGURE 31: Percentage improvement with totally variable length system

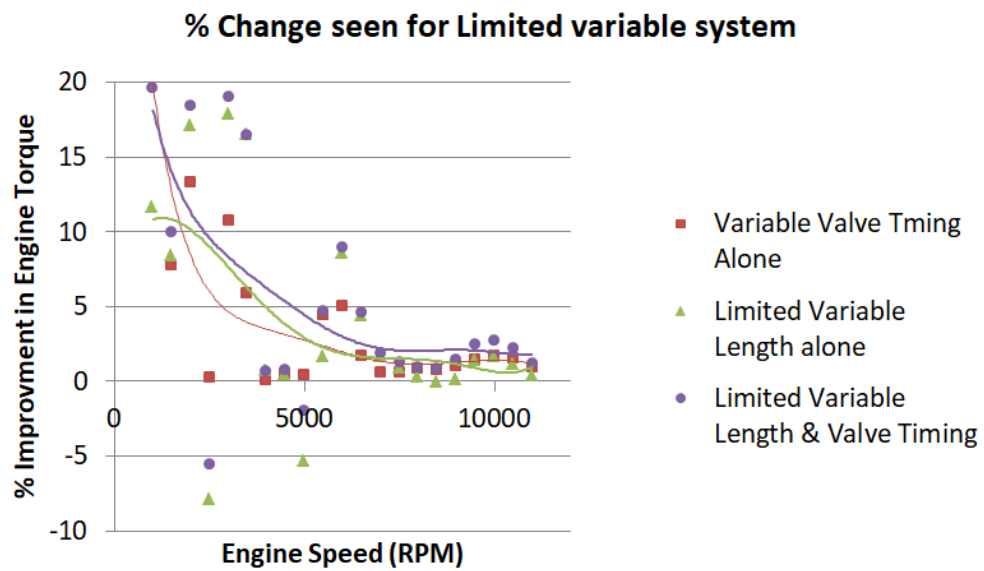


FIGURE 32: Percentage improvement with limited variable length system

3.2. BASIS FOR FURTHER STUDY

On further research, combined effect of runner length variation along with valve timing has shown promising results. In earlier study, the valve timing was varied with the runner length kept constant, but at an optimized setup. However, more research showed a pattern in the combined variation of the two parameters. The study of these patterns indicated that the runner length and valve timing as a combination yields higher results than the former method employed. To arrive at this point, the exhaust runner length is varied again along with the exhaust valve timing. Based on the results seen new case setup was decided upon as discussed above in case setup. The effects of the valve lift were studied in addition to the combination of the runner length and valve timing. More in depth results of runner length effects and valve timing are discussed in the following sections.

3.2.1. VARIATION OF RUNNER LENGTH

For the 2nd stage case setup made, plotting the engine torque values for different runner lengths and engine speeds generated a surface plot as shown in Figure 33. The values can be seen to be high at light colored regions. These peak areas marked 1 and 2 in Figure 33 indicate the maximum performance that can be achieved with different runner lengths and thus should be the target region. Figure 34 shows the engine torque values for an engine speed of 3000 RPM. These values can be seen to increase and decrease as the runner length changes. The values rise to a peak and then drop. This repeats several times and each time, the height of the peak increases and then drops to a lower value. To explain this behavior, the pressure traces near the exhaust port are observed.

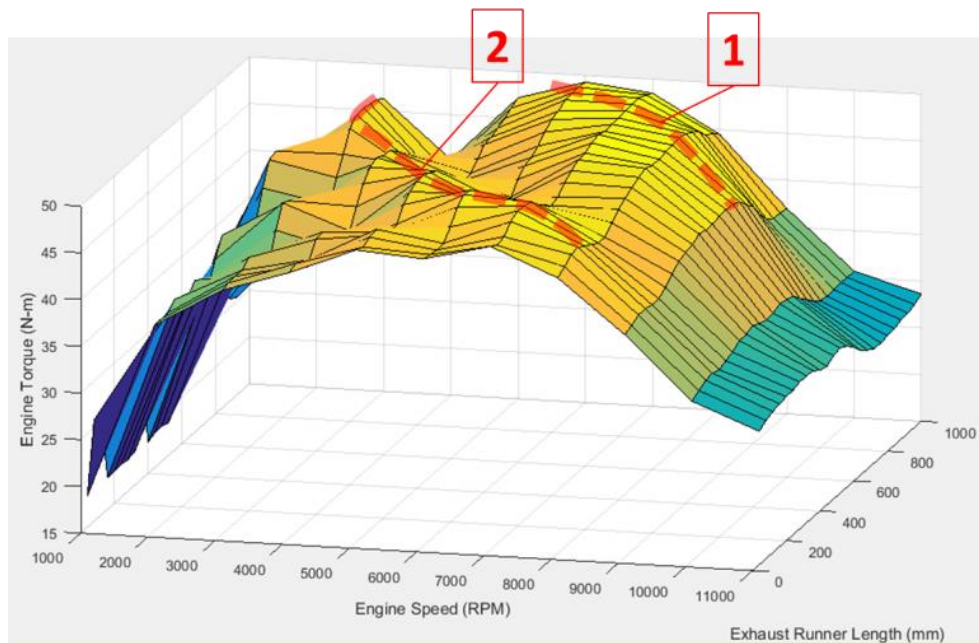


FIGURE 33: Engine torque (Nm) Vs Runner length (mm) and Engine speed (RPM)

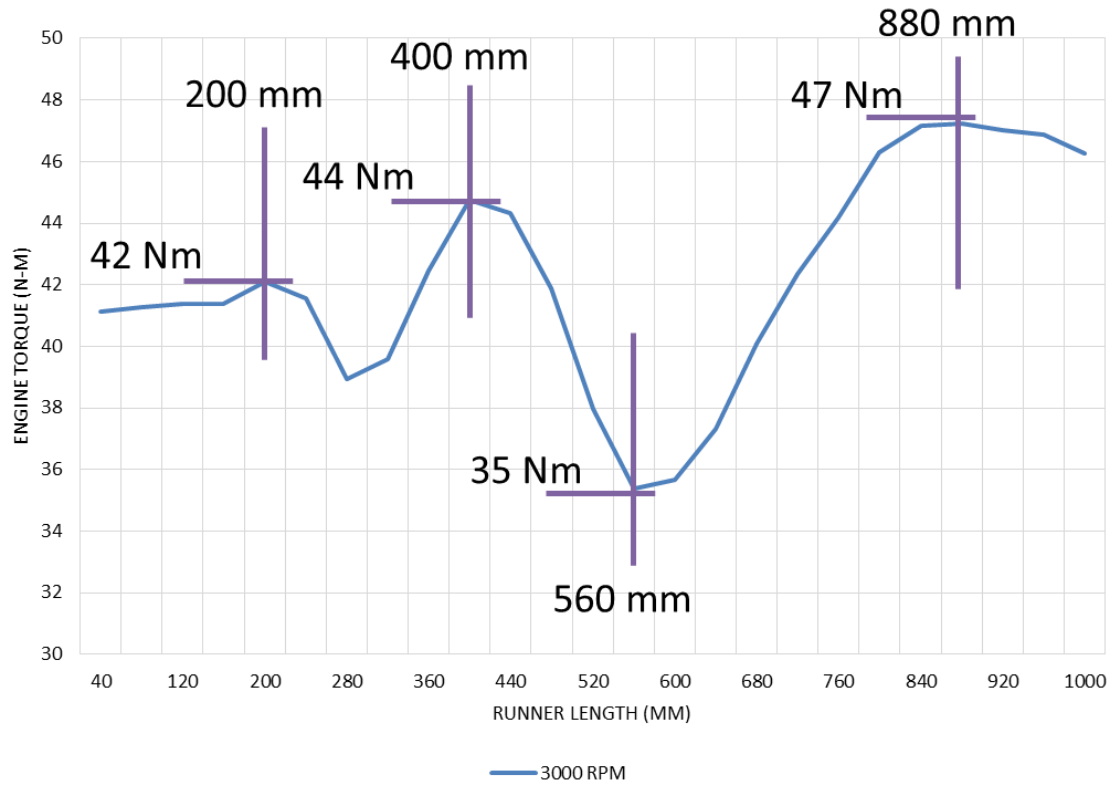


FIGURE 34: Engine torque (Nm) Vs Runner length for 3000 RPM

Figure 35 shows the pressure values of the exhaust gases at a distance of approximately 9 mm downstream of the exhaust valve in the exhaust port. As the exhaust valve opens, the high pressure in the combustion chamber starts rushing out of the exhaust valve. This creates a local high pressure zone. This high pressure zone flows as a pressure wave through the runner. The speed of this wave is equivalent to the speed of sound given by Equation (1) in earlier sections.

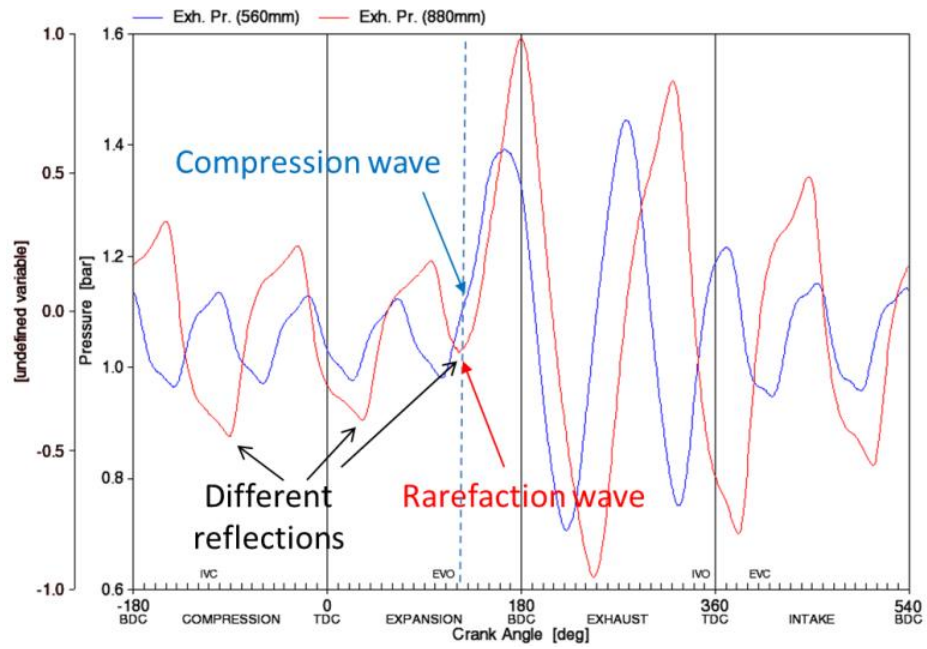


FIGURE 35: Pressure traces at approx. 9mm downstream from exhaust valve for the two runner lengths

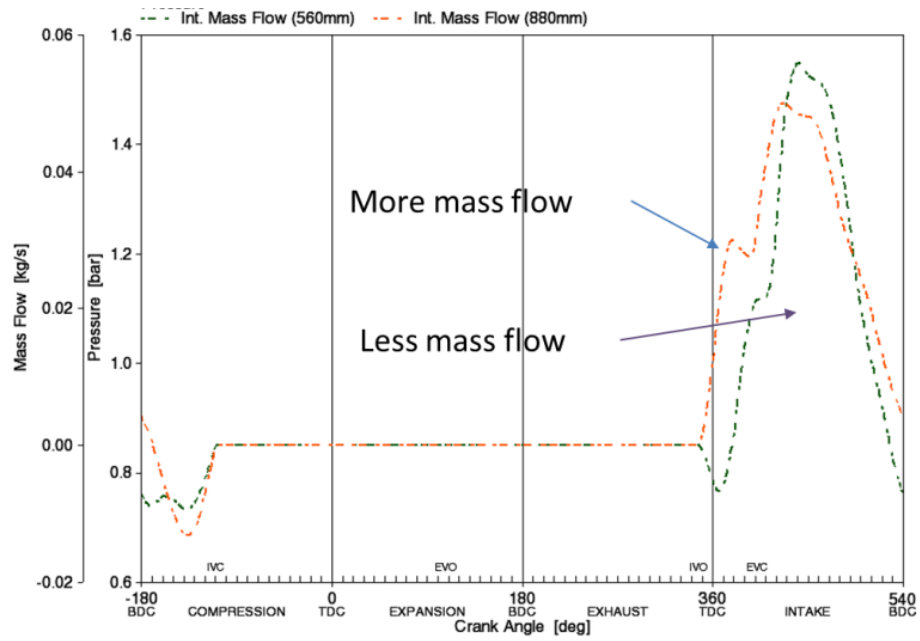


FIGURE 36: Intake mass flow rate (kg/s) for the two runner lengths

As per the physics of compression waves in tubes, the waves flow until they see a change in flow area. As the high pressure wave, also known as compression wave, created at the exhaust valve reaches the end of the runner, it reflects and starts to flow back towards the exhaust valve. However, since the flow area changed when the wave reflected, it converts from a high pressure wave to a low pressure wave as per the physics of pressure waves. The low pressure waves are also called rarefactions. The rarefaction wave travels back to the exhaust valve. If the exhaust valve is closed, it reflects against the valve. Since there is no change in the flow area at the exhaust valve, the rarefaction remains as a rarefaction wave and starts travelling back to the end of the runner. The rarefaction wave reflects at the end of the runner and changes to a compression wave as there is change in flow area. The compression wave travels back to the exhaust valve and reflects as a compression wave if the exhaust valve remains closed. This repeats until the exhaust valve opens. These reflections keep changing between rarefactions and compression waves at the end of the runner and will keep reverberating until the exhaust valve opens again.

In Figure 35, the peaks represent compression waves and the negative peaks represent rarefactions at 9 mm distance to exhaust valve in the exhaust port. The pressures in the two different cases can be observed in relation to the EVO, marked by the dashed line. The pressure is at approximately 1.1 bar and 1.0 bar for 560 mm and 880 mm runner length respectively. The lower pressure value for 880 mm created a high pressure differential between the exhaust port and combustion chamber which helped in better evacuation of the exhaust gases when the exhaust valve opened. In addition, at valve overlap, that is when inlet valve opens and before the exhaust valve closes, the

pressure was 1.2 bar and 0.7 bar for 560 mm and 880 mm runner length respectively. Figure 36 shows the intake mass flow rate for the two cases. The mass flow rate at valve overlap drops to a negative value for 560 mm runner length, indicating that there was reverse flow from the intake valve. On the other hand, a steep rise was seen in mass flow rate at valve overlap for 880 mm runner length. The low pressure for 880 mm runner length as compared to that of 560 mm runner length enabled better suction of the intake charge into the combustion chamber. Though the mass flow rate for 560 mm runner length picked up after sometime and rises to a high peak value the area under the curve was less than that of 880 mm runner length. This indicated that the intake mass flow was much better for 880 mm runner length. These lead to a higher volumetric efficiency and thus better engine torque.

Table 4 shows the mass flow rate for the two cases. The mass flow rate was about 30% more for 880 mm runner length compared to 560 mm runner length. The residual gas fraction was as low as 1.2 % for 880 mm against 8.8 % for 560 mm runner length. This indicated that the exhaust gas evacuation was near 100% for 880 mm. The volumetric efficiency was as high as 93.6 % for 880 mm, whereas, it was only 69.9 % for 560 mm runner length. Figure 35, Figure 36 and Table 4 show that the scavenging efficiency increases when the EVO faces a rarefaction wave as compared to a compression wave. Therefore the runner length had to be tuned in such a way that the rarefaction wave reaches when exhaust valve opens.

TABLE 4: Comparison of exhaust gas flow for 560 mm and 880 mm runner lengths for 3000 RPM

	560 mm	880 mm
Mass flow rate (kg/hr)	37.4	50.1
Residual gas fraction (%)	8.8	1.2
Scavenging efficiency (%)	91.2	98.8
Volumetric efficiency (%)	69.9	93.6

3.2.1.1. REFLECTIONS AND PULSE STRENGTH

If the exhaust valve stays closed when the first rarefaction wave returns from the end of the runner, the rarefaction reflects against the valve and at the end of the runner converts to a compression wave. The compression wave reflects against the closed exhaust valve and returns to the runner end, where it converts to a rarefaction wave. Therefore, the engine torque value will peak again for this 3rd reflection (or 2nd rarefaction wave) if the exhaust valve opens for this reflection. Figure 34 also shows two more peaks at 200 mm and 400 mm runner length. These two peaks represent the engine torque achieved for reflected rarefaction waves. However the values at these peaks reduce for each reflection. This is since for every reflection the pressure of these waves increase (rarefaction wave are low pressure waves). The pressure is the strength for these waves and lesser the pressure (for rarefaction waves), higher is its strength in improving scavenging efficiency. Figure 35 shows that the pressure raised by about 0.1 bar for every

reflection. For a runner length of 400 mm, the engine torque dropped by 3 Nm as compared to 880 mm runner length, which was about 6 %. Engine torque dropped another 2 Nm for 200 mm runner length which totaled to a 10 % drop. Therefore, it was highly beneficial to take advantage of the earliest reflection that was possible.

3.2.1.2. RUNNER LENGTH SELECTION

The target to achieve maximum performance was to select the runner length such that the rarefaction wave reaches in accordance to the exhaust valve opening. The earliest reflection has higher pulse strength and thus yields maximum benefit. However, as seen from the equations given by Blair et al. and Bell et al, the runner length requirements increases exponentially as the engine speed decreases. It becomes difficult to package runner lengths beyond 1000 mm. From Figure 1, it can be seen that the 1st rarefaction reflection can be achieved only for engine speeds as low as 6000 RPM. For lower engine speeds later reflections have to be used.

Similar to figure 20, for every engine speed, when the engine torque achieved was deducted from the maximum possible engine torque at that engine speed, figure 37 was obtained. The 1st and 2nd rarefaction reflections are marked with black lines. These dark regions, where the deficit is less, are the target areas to achieve maximum engine performance. Similar to the curves seen in Figure 1, the runner length requirements curve from about 300 mm for 11000 RPM to about 1000 mm for 6000 RPM. The 2nd rarefaction zone curves from about 200 mm at 8000 RPM to 1000 mm at 3000 RPM.

Packing constraints would be different for different vehicles. If 800 mm was assumed to be the limit for this case, the runner length was sufficient for 1st rarefaction reflection only from 7000 RPM to 11000 RPM. Therefore, later rarefaction reflections had to be used for speeds below 7000 RPM. Figure 37 shows the possible runner sequence, marked in dotted white line, that can be followed such that 1st rarefaction reflection was used for speeds 7000 to 11000 RPM and later reflections for lower engine speeds. Assuming a telescopic system of runner length variation, the runner length can only change at a certain rate and cannot change instantaneously from one length to another. Therefore, as the runner length shifts from 1st to the 2nd rarefaction reflection, the sequence will fall into the compression wave region (marked in dashed white line in Figure 37). As the runner lengths fall under the compression wave zone, the scavenging efficiency drops and the engine torque values are at low values as understood from the theory of compression waves above. For the runner length sequence chosen in Figure 37, the engine torque curve can be compared against the actual curve and is shown in Figure 38.

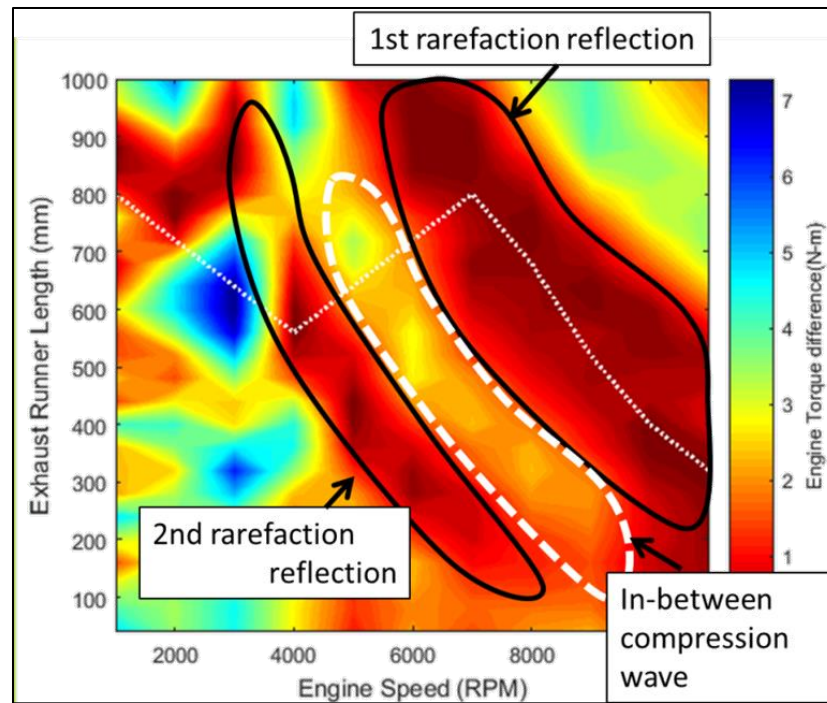


FIGURE 37: Difference of maximum and achieved engine torque at runner length for each engine speed

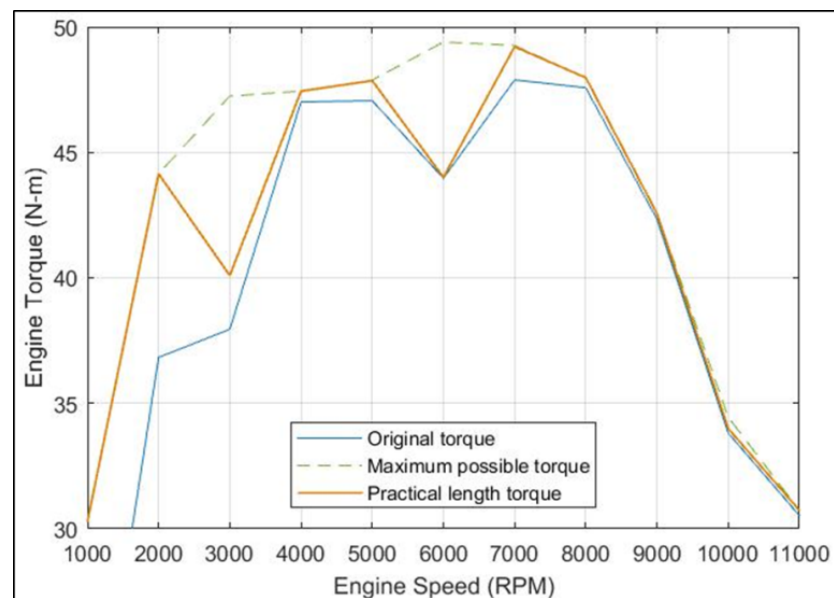


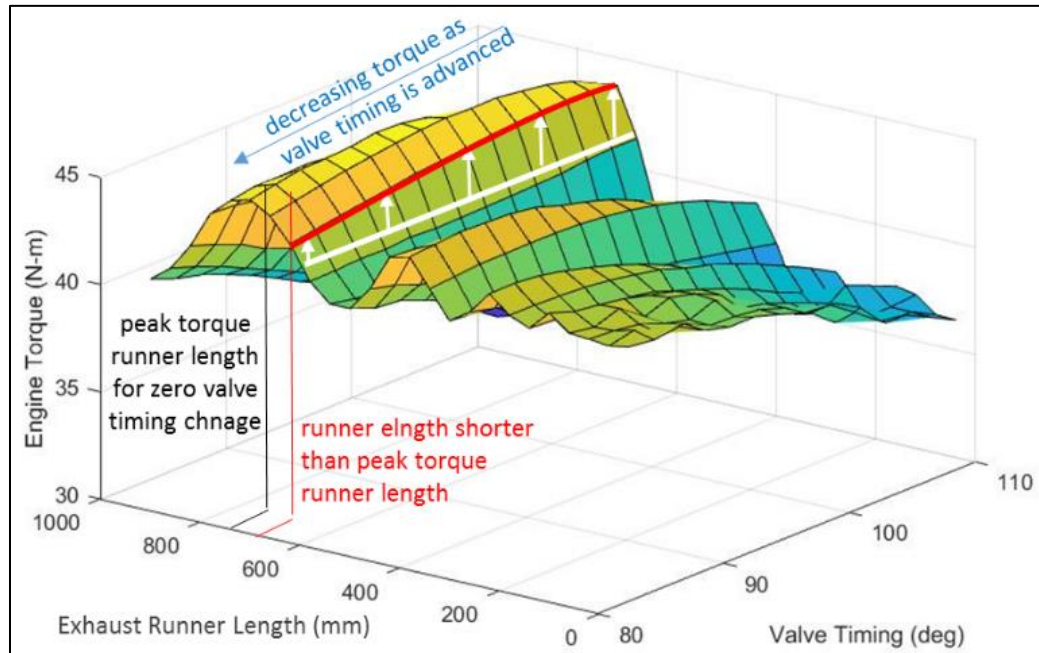
FIGURE 38: Engine torque for variable sequence runner length

Figure 38 shows the engine torque curve for the actual runner length of 520 mm, maximum possible engine torque with fully variable runner length and the engine torque curve that can be achieved with the runner length sequence as shown in Figure 37. The engine torque values at 3000 RPM and 6000 RPM are low as compared to the maximum possible engine torque at those engine speeds as for the runner length sequence chosen, they pass through the compression wave zone.

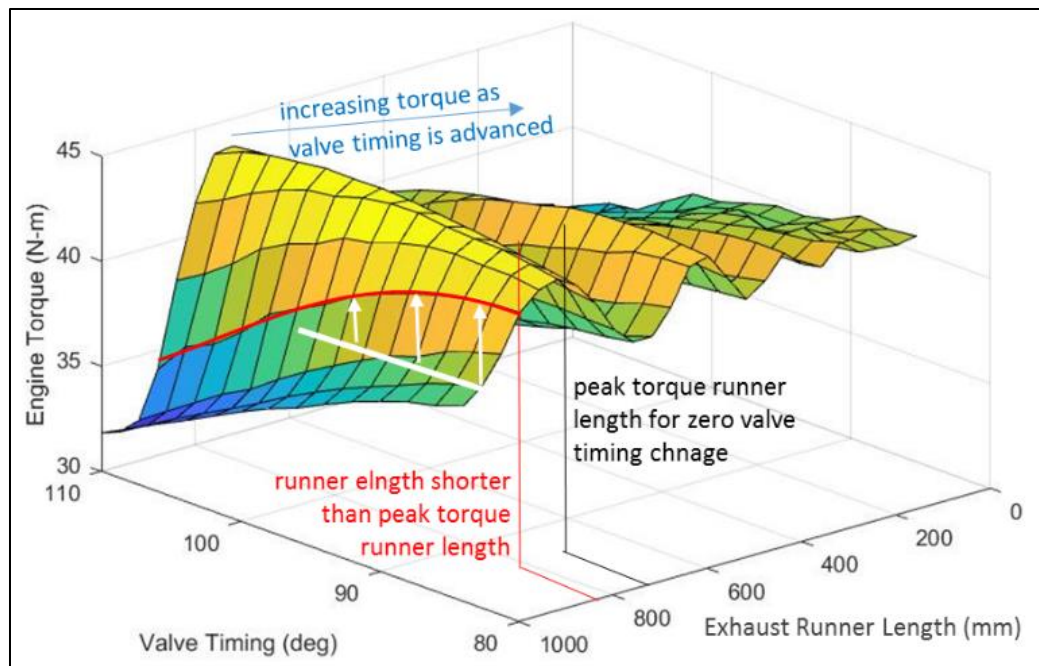
3.2.2. VARIATION OF VALVE OPENING TIME AND LIFT

In addition to the exhaust runner length, the exhaust valve operating conditions are also major contributors to the performance of the engine. If the engine torque is plotted against both exhaust runner length and exhaust valve timing, the relative variations of the two factors can be observed. Figure 39 shows the 3D surface plot for the engine torque values at 2000 RPM. The peak torque was observed at 760 mm for 2000 RPM when the runner length alone was varied. One important observation was the type of variation that the engine torque showed as the exhaust valve timing was advanced near the 760 mm runner length region. From Figure 39 (a), it can be observed that the neighboring shorter runner lengths to 760mm see a decrease in engine torque values as the valve timing is advanced from 110° aTDC to 84° aTDC. Whereas, Figure 39 (b) shows the neighboring longer runner lengths to 760mm to see an increase in engine torque values as the valve timing was advanced from 110° aTDC to 84° aTDC.

Therefore, it was important to check the exhaust valve timing for runner lengths near the peak region to arrive at the best combination of runner length and valve timing.



(a)



(b)

FIGURE 39: 3D surface plot of engine torque for engine speed of 2000 RPM

The variation of engine torque values at the peak torque runner length of 760 mm started to increase as the valve timing was advanced and then started to drop. The engine torque curves at these areas if plotted as 2D curves, by keeping the runner length constant and by varying the exhaust valve timing, the variation can be seen clearly. Figure 40 shows the engine torque values at 760mm, shorter runner length of 640 mm and longer runner length of 840 mm for 2000 RPM. As the exhaust valve timing is advanced from 100° aTDC to 84° aTDC the engine torque values decreased for 640 mm, increased and then decreased for 760 mm and increased for 840 mm. It can be said that the combination is optimum when the rarefaction arrives in accordance to EVO. Both runner length and EVO tend to peak towards these values and then drop again. Therefore, it is critical to check the performance with both parameters varied at once. The same trend is observed at all engine speeds but at different magnitudes. However if the peak performance values are checked for all engine speeds, it can be observed that as the engine speed increases, the valve opening time was required to be advanced. The valve duration of 300 degrees was covered in approximately 8 ms for 3000 RPM and 4 ms for 6000 RPM. Since the time for evacuation reduces considerably as engine speed increases the exhaust valves need to open earlier to allow more pressure differential to expel the exhaust gases efficiently.

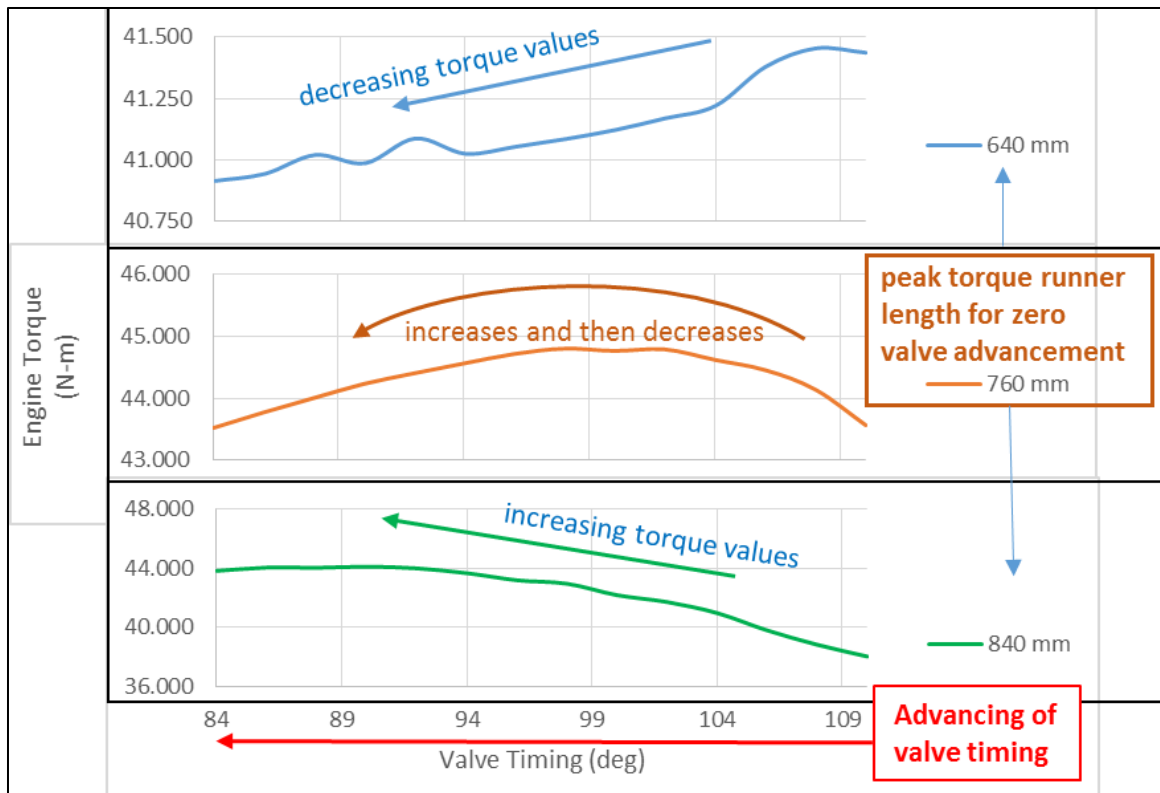
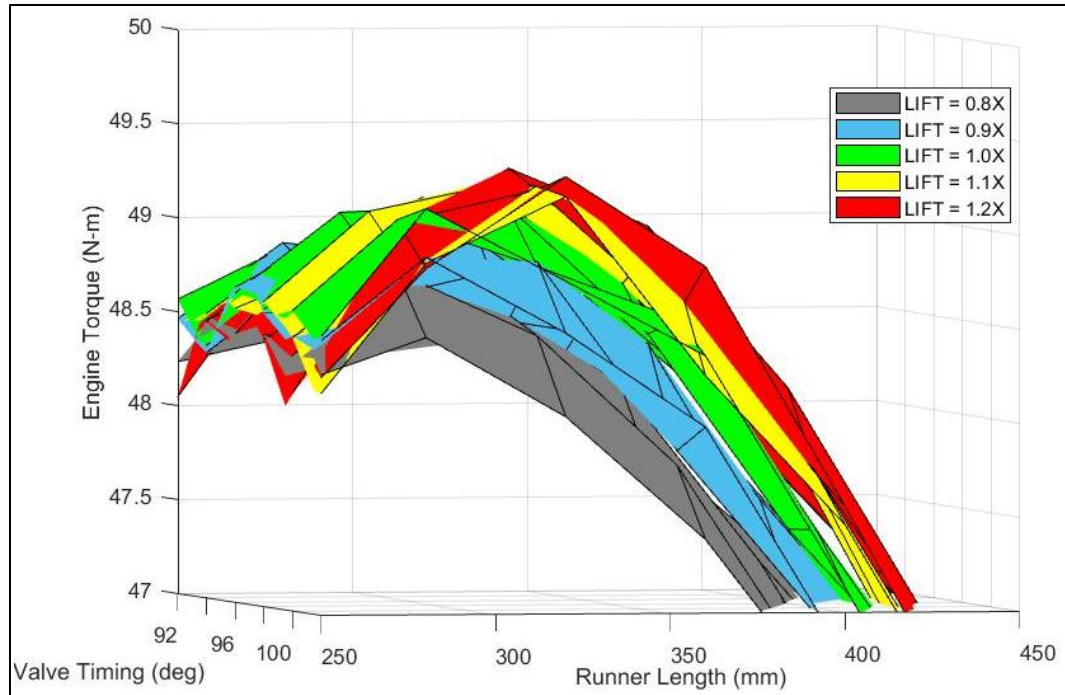
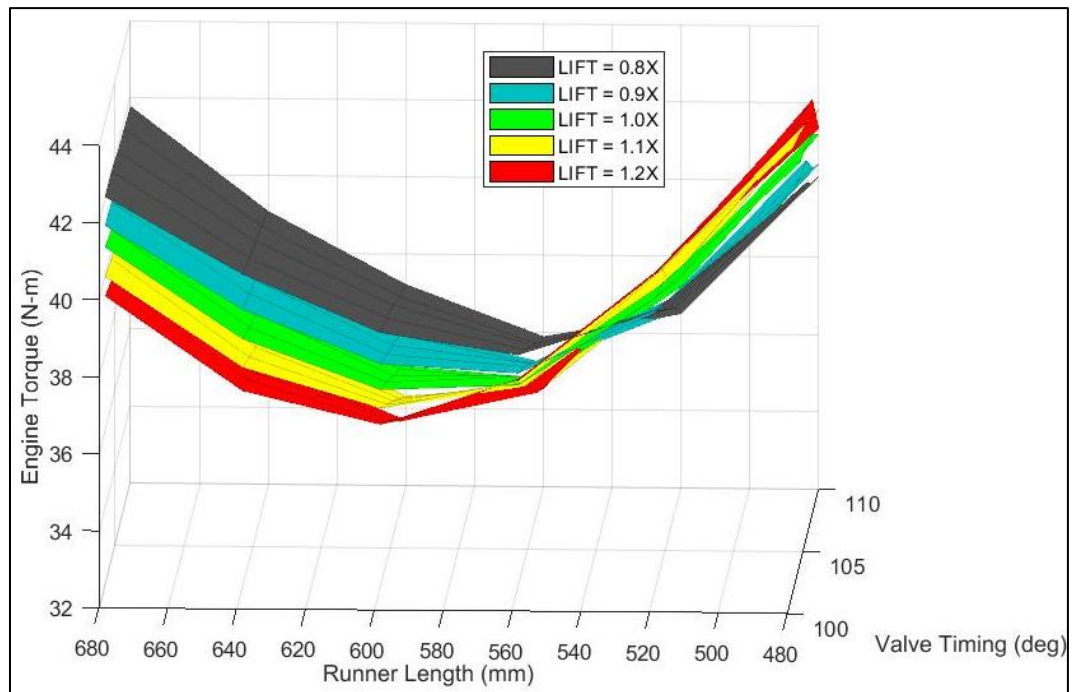


FIGURE 40: Engine torque variation with changes in valve timing for engine speed of 2000 RPM for different runner lengths

The variation of valve lift from 0.8X to 1.2X for 7000 rpm is shown in Figure 41. It is well known that as the valve lift is increased, the flow area for the exhaust gases is increased and thus better scavenging takes place. As the lift was increased for the peak values in the engine torque curves seen, shown in Figure 41(a), the 3D surface plots shift up and towards longer runner length. Increase of valve timing by 0.2X increases engine torque by about 0.5 %. However, the most important aspect of variation of lift was to compensate for the loss of torque seen when the runner length was in the range of compression wave. By limiting the valve lift the negative effect of the compression wave acting against the exhaust gas flow was reduced. Figure 41 b) shows the engine torque values at the compression wave zone for valve lifts from 0.8X to 1.2X. As the lift was decreased, the engine torque values increased. In other words, the loss of engine torque or the negative effect was reduced.



(a)



(b)

FIGURE 41: Variation of engine torque with variation of valve lift for 7000 RPM

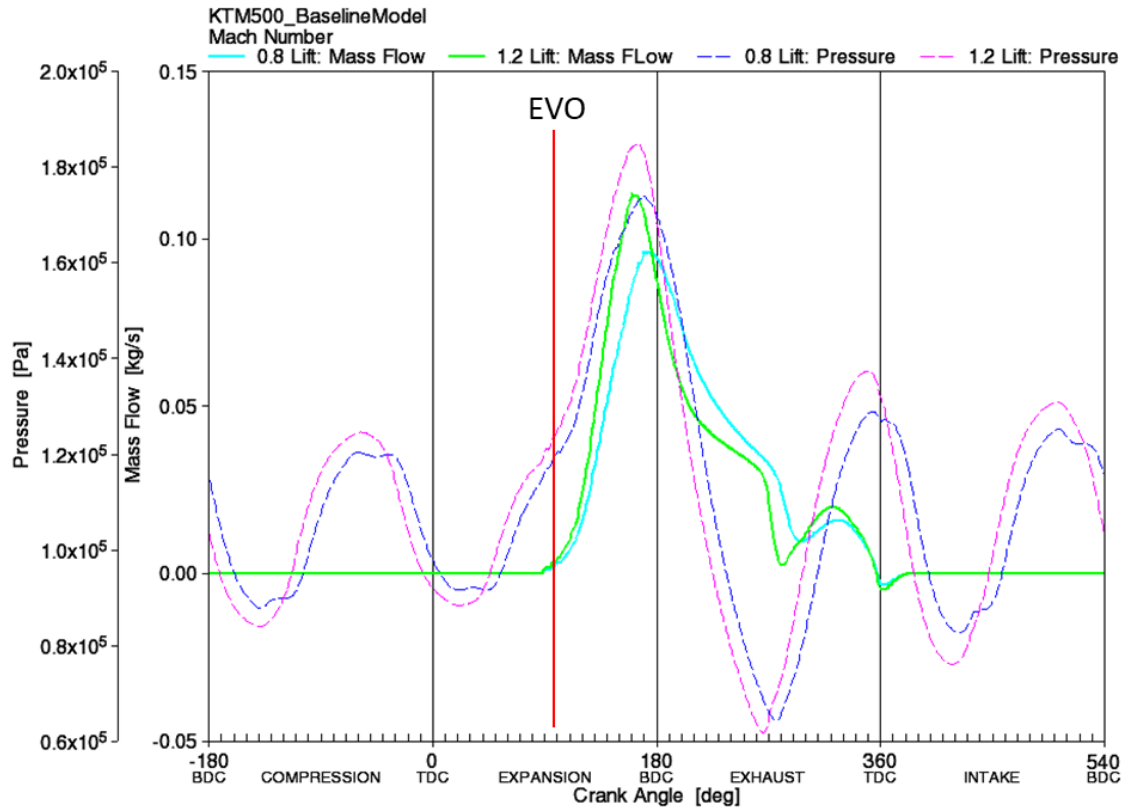


FIGURE 42: Pressure traces 9 mm downstream of exhaust valve and mass flow rate at exhaust valve for 7000 RPM for valve lift of 0.8X and 1.2X

Figure 42 shows the pressure traces 9 mm downstream of exhaust valve and mass flow rate at exhaust valve for 7000 RPM for valve lift of 0.8X and 1.2X. With 1.2X valve lift, the pressure as the exhaust valve opened was slightly higher. The exhaust gas pressure rose steeply to about 1.85 bar and the exhaust gas mass flow rate also rose to about 1.1 kg/s. However the mass flow rate quickly dropped. Whereas, for the valve lift of 0.8X, the pressure at exhaust valve opening was slightly lower comparatively. With the lift profile scaled down by 0.4X, the valve opening was more gradual than that of 1.2X valve lift. The mass flow rate rose more gradually and although it did not peak as

high as 1.2X valve lift, the mass flow rate dropped more gradually, allowing more exhaust gases to flow. The area under the mass flow rate curve for 0.8X was much higher than that of 1.2X valve lift. Due to this, the lower valve lift was controlling the negative effect of higher pressure from the runner and allowing better scavenging.

3.2.3. IMPROVEMENTS

Figure 43 shows the engine torque curves from 1000 RPM to 11000 RPM for the actual engine setup and variable exhaust system. Due to possible practical limitations for exhaust runner length variation, it was observed that the scavenging performance was low at 3000 RPM and 6000 RPM. However, with variable exhaust valve timing and lift, this loss was recovered. Figure 43 shows that the possible engine torque achievable are 47 Nm and 49 Nm at 3000 RPM and 6000 RPM respectively. However, due to practical limitations, the engine torque achieved was only 42 Nm and 46.5 Nm for 3000 RPM and 6000 RPM respectively. This loss was recovered by 50% or in other words, the original torque can be improved by 50% of the maximum possible torque by taking benefit of the variation of valve timing and lift. The combined benefit of a variable length, variable valve timing and lift system the gain in improvement is significant. It can be seen that the actual runner length of 520 mm benefited the high engine speeds. Therefore, the improvement seen from 8000 RPM to 11000 RPM is less and the improvements possible at lower engine speeds are high. However, the engine torque can improve by about 3% due to variable valve timing and lift. Figure 44 shows the percentage improvement for the engine torque curves shown in Figure 43. The possible improvement was 24 % and

12 % at 3000 RPM and 6000 RPM respectively. However, due to practical limitations discussed, this cannot be achieved with just the runner length change as per the sequence. With variable valve timing and lift, 11 % and 6 % were achieved for 3000 RPM and 6000 RPM respectively, which was approximately 50 % of the achievable improvement.

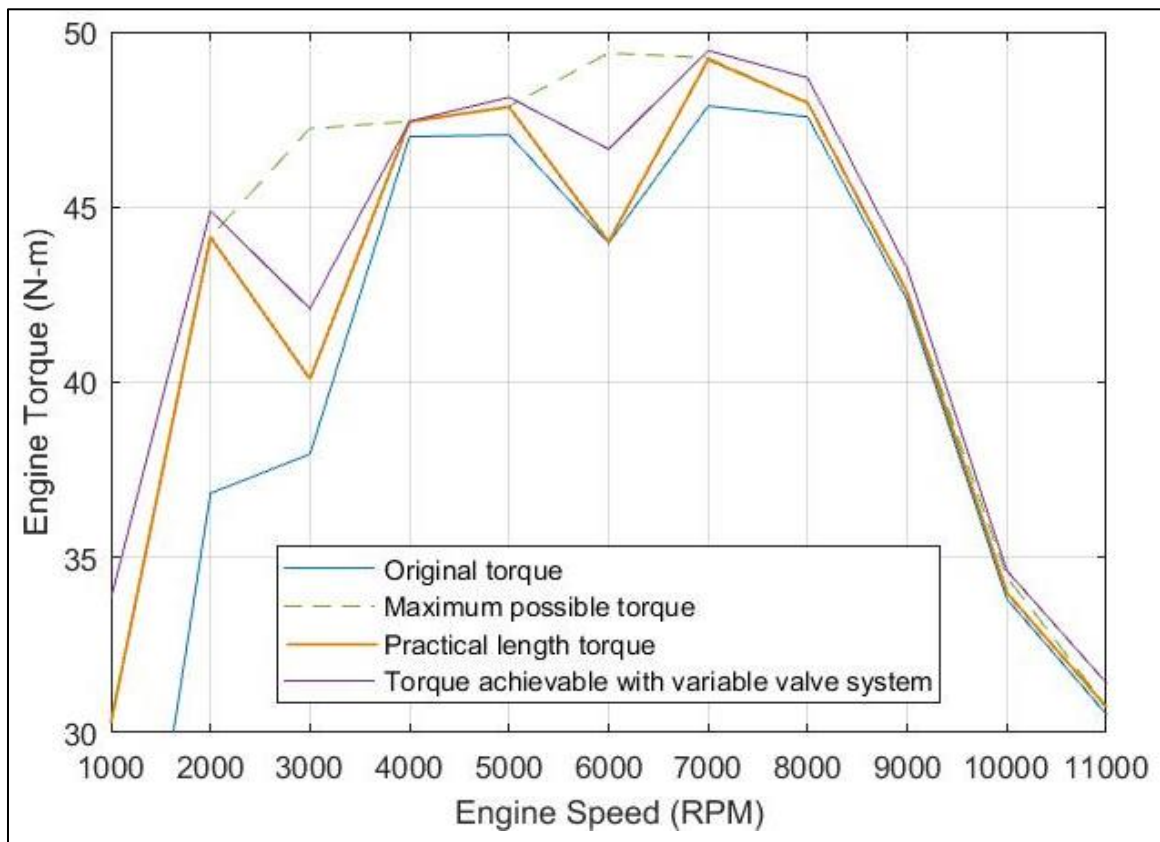


FIGURE 43: Engine Torque improvements with exhaust valve timing and lift

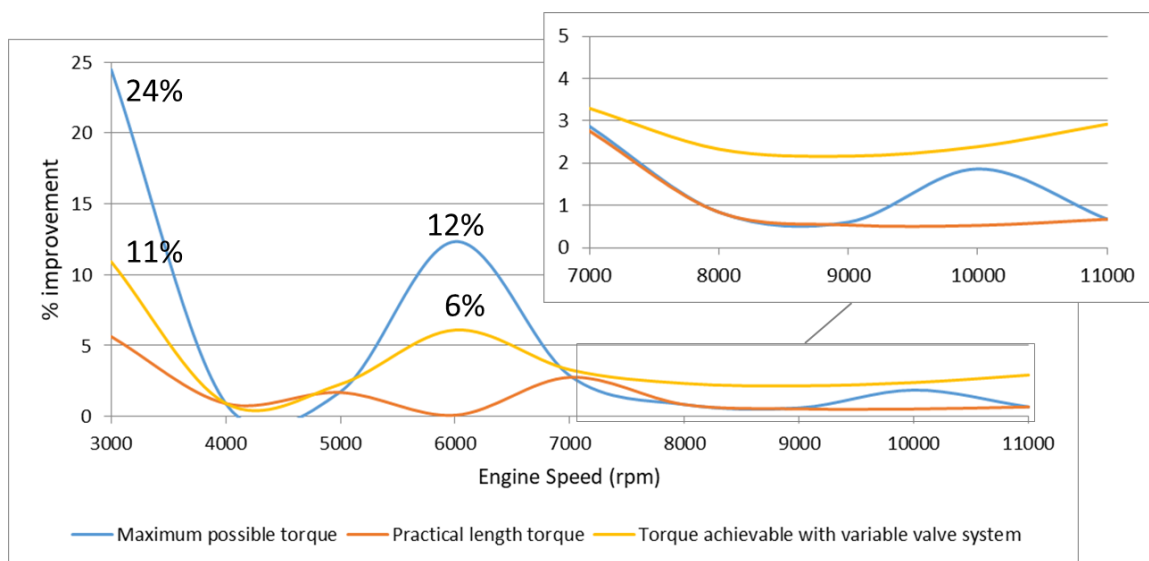


FIGURE 44: Percentage improvements with variable exhaust system

4. CONCLUSION

It was observed that the scavenging efficiency of the exhaust system had an effect on the volumetric efficiency of the engine. The scavenging efficiency of the exhaust system when improved, the pressure differential increased between the combustion chamber and exhaust runner and thus higher volumetric efficiency was achieved. At EVO, a high pressure wave was observed to start and reverberate through the runner and change sign every time the flow area changed. The alternating rarefaction and compression waves influenced the scavenging efficiency of the engine. Based on these principles, the runner length and valve train were tuned to take benefit of the rarefaction waves to improve the scavenging efficiency. This in turn improved the volumetric efficiency and thus the performance of the engine.

It was found that simulation tools are cost and time effective and yield highly accurate results without the effort of physical work. 1-D model analysis gave detailed results for understanding the behavior of runner length, valve timing and valve lift on the effect of pressure waves. The runner length requirement varies at different engine speeds. The exhaust gases been very hot, the pressure waves travel at a very high speed and therefore the reflection time for one reflection was found to be very small. At high engine speeds, as the time between EVO events is small, the small reflection time was used with short runner lengths. However at lower engine speeds, to cater for the small reflection times, the runner length had to be increased massively, which was not possible due to space limitations. To keep the runner lengths within limits, later reflections had to be used. As the pulse strength decreases for every reflection, it was ideal to stick with the earliest reflections where possible and shift to later reflections for lower engine speeds.

The runner length tuning was easier at high engine speeds but had narrow tuning bands at lower engine speeds. At 7000 RPM, 90% of peak torque was achieved within a wide band of 250 mm for the 1st reflection. Whereas, at 3000 rpm, 90% peak torque was limited to 50 mm for the 2nd reflection. To gain maximum benefit a variable runner length proved beneficial and therefore, a telescopic type of runner length variation was recommended. Shifting of the runner length from one reflection to another was unavoidable for a single variable runner length system. Such a system, which had to shift to later reflections as the engine speed decreases, suffered in performance in the shifting zones.

A combination of runner length and valve timing had shown a pattern which helped in understanding the combined effect. The runner length and valve timing converged to a point, where the maximum performance was obtained. The study of this pattern was important as it lead to the understanding of the relation of rarefaction waves with advancement of valve opening time with engine speed and the runner length. The exhaust valve opening time had to be advanced from 3000 RPM as the exhaust gases need more time to evacuate at higher engine speeds. Valve timing also affected the runner length requirement and improved the engine torque by about 1-2% at lower engine speeds and little to no improvement at higher engine speeds. The combined improvement with tuned length and valve timing was in the range of 5-8% and 1-2% at lower and higher engine speeds respectively. For the runner length variation, as the shift makes the sequence flow through the compression wave zone, the performance was very low at 3000 RPM and 6000 RPM. The increase in valve lift enabled for better flow area when the exhaust gases were flowing out of the combustion chamber. Increase in valve lift by

20% benefited the engine torque at the rarefaction wave zone by about 1.5%. However, it was observed that limiting the valve lift reduced the negative effect of the compression wave. When the compression wave returns at EVO, it hinders the flow, therefore, limiting the valve lift did not affect the exhaust flow, but rather reduced the negative force of the compression wave and allowed for more gradual exhaust gas evacuation. With tuned valve timing and 20% less valve lift the loss of performance seen at the compression wave was reduced by almost 50%. Exhaust system contributed to an overall improvement in engine torque performance by about 2-3% and 7-10% at higher and lower engine speeds respectively.

REFERENCES

1. Benajes, J., et al., *Pre-design criteria for exhaust manifolds in IC automotive engines*. 1998, SAE Technical Paper.
2. Kesgin, U., *Study on the design of inlet and exhaust system of a stationary internal combustion engine*. Energy Conversion and management, 2005. **46**(13): p. 2258-2287.
3. Malkhede, D.N. and H. Khalane, *Maximizing Volumetric Efficiency of IC Engine through Intake Manifold Tuning*. 2015, SAE Technical Paper.
4. Thompson, M.P., *Non-mechanical supercharging of a four-stroke diesel engine*. 1968, The Ohio State University.
5. Manual, D., *Users Guide and Engine Builder's Handbook*, in *Dynomation5 Professional* 1995.
6. Tabaczynski, R.J., *Effects of Inlet and Exhaust System Design on Engine Performance*. 1982, SAE International.
7. Baechtel, J., *Performance Automotive Engine Math*. 2011: CarTech.
8. Blair, G.P., *Design and simulation of engines: a century of progress*. 1999, SAE Technical Paper.
9. Schweitzer, P.H., *Scavenging of two-stroke cycle diesel engines*. 1949: Macmillan Co.
10. Ricardo, H.R., *The high-speed internal-combustion engine*. 1953.
11. Bell, A.G., *Four-stroke performance tuning*. 1998: Cambridge University Press.

12. Hamilton, L.J., J. Cowart, and J. Rozich, *The Effects of Intake Geometry on SI Engine Performance*. 2009, SAE Technical Paper.
13. Blair, G.P., *Design and Simulation of Four-Stroke Engines*. Technology, 1999. **2011**: p. 10-18.
14. Ibrahim, A., S. Bari, and F. Bruno, *A study on EGR utilization in natural gas SI engines using a two-zone combustion model*. 2007, SAE Technical Paper.
15. Blair, G.P., et al., *Exhaust tuning on a four-stroke engine; experimentation and simulation*. 2001, SAE Technical Paper.
16. Bari, S. and I. Saad. *Effects of guide vane swirl and tumble device (GVSTD) to the air flow of naturally aspirated CI engine*. 2011. ICME.
17. Saad, I. and S. Bari, *Optimize vane length to improve in-cylinder air characteristic of CI engine using higher viscous fuel*. Vol. 393. 2013: Trans Tech Publ.
18. Baechtel, J., *Practical Engine Airflow : Performance Theory and Application*. 2015.
19. Heywood, J.B., *Internal combustion engine fundamentals*. Vol. 930. 1988: McGraw-hill New York.
20. Vizard, D., *David Vizard's holley carburetors: how to super tune and modify*. 2013: CarTech.
21. Engelman, H.W., *Design of a tuned intake manifold*. ASME paper, 1973(73-WA).
22. Bell, A.G., *Performance tuning in theory and practice: four strokes*. 1981: Haynes.

23. Sammut, G. and A.C. Alkidas, *Relative contributions of intake and exhaust tuning on SI engine breathing-A computational study*. 2007, SAE Technical Paper.
24. Ohata, A. and Y. Ishida, *Dynamic inlet pressure and volumetric efficiency of four cycle four cylinder engine*. 1982, SAE Technical Paper.
25. Bush, P., et al., *A design strategy for four cylinder SI automotive engine exhaust systems*. 2000, SAE Technical Paper.
26. Winterbone, D. and M. Yoshitomi, *The accuracy of calculating wave action in engine intake manifolds*. 1990, SAE Technical Paper.
27. Silvestri, J.J., T. Morel, and M. Costello, *Study of intake system wave dynamics and acoustics by simulation and experiment*. 1994, SAE Technical Paper.
28. Deshmukh, D., et al., *Optimisation of gas exchange process on a single cylinder small 4-stroke engine by intake and exhaust tuning: Experimentation and simulation*. 2004, SAE Technical Paper.
29. Claywell, M., D. Horkheimer, and G. Stockburger, *Investigation of intake concepts for a formula SAE four-cylinder engine using 1D/3D (Ricardo WAVE-VECTIS) coupled modeling techniques*. 2006, SAE Technical Paper.
30. Thomke, S.H., *Simulation, learning and R&D performance: Evidence from automotive development*. Research Policy, 1998. **27**(1): p. 55-74.
31. Saad, I., S. Bari, and S.N. Hossain, *In-cylinder air flow characteristics generated by guide vane swirl and tumble device to improve air-fuel mixing in diesel engine using biodiesel*. Procedia Engineering, 2013. **56**: p. 363-368.

32. Saad, I. and S. Bari, *Improving air-fuel mixing in diesel engine fuelled by higher viscous fuel using guide vane swirl and tumble device (GVSTD)*. 2013, SAE Technical Paper.
33. Khoo, A.S., *Simulation And Experimental Studies Of Intake And Exhaust Tuning For Automotive Engine Low-End Torque Enhancement*. 2014, Universiti Sains Malaysia.
34. Software, R., *WAVE Knowledge Center*. 2015.
35. Manual, O.s., *Owner's Manual 500 EXC US*. 2015.
36. Liu, Y.C., A.J. Savas, and C.T. Avedisian, *Comparison of the burning characteristics of indolene and commercial grade gasoline droplets without convection*. *Energy & Fuels*, 2012. **26**(9): p. 5740-5749.
37. Gajula, V. and S. Bari. *Performance tuning of an IC engine based on pressure wave propagation with a continuously variable exhaust runner length and exhaust valve timing system*. in *ASME 2017 International Mechanical Engineering Congress and Exposition*. 2017. Tampa, FL, USA: ASME.